



**Pacific Northwest**  
NATIONAL LABORATORY

*Proudly Operated by Battelle Since 1965*

# Identify and Quantify the Mechanistic Sources of Sensor Performance Variation Between Individual Sensors SN1 and SN2

M3AR-14PN2301022 Technical Letter Report

**July 2014**

AA Diaz  
DL Baldwin  
AD Cinson  
AM Jones  
MR Larche  
RA Mathews

CA Mullen  
AF Pardini  
GJ Posakony  
MS Prowant  
TS Hartman  
MK Edwards

## DISCLAIMER

This report was prepared as an account of work sponsored by an agency of the United States Government. Neither the United States Government nor any agency thereof, nor Battelle Memorial Institute, nor any of their employees, makes **any warranty, express or implied, or assumes any legal liability or responsibility for the accuracy, completeness, or usefulness of any information, apparatus, product, or process disclosed, or represents that its use would not infringe privately owned rights**. Reference herein to any specific commercial product, process, or service by trade name, trademark, manufacturer, or otherwise does not necessarily constitute or imply its endorsement, recommendation, or favoring by the United States Government or any agency thereof, or Battelle Memorial Institute. The views and opinions of authors expressed herein do not necessarily state or reflect those of the United States Government or any agency thereof.

PACIFIC NORTHWEST NATIONAL LABORATORY  
*operated by*  
BATTELLE  
*for the*  
UNITED STATES DEPARTMENT OF ENERGY  
*under Contract DE-AC05-76RL01830*

Printed in the United States of America

Available to DOE and DOE contractors from the  
Office of Scientific and Technical Information,  
P.O. Box 62, Oak Ridge, TN 37831-0062;  
ph: (865) 576-8401  
fax: (865) 576-5728  
email: reports@adonis.osti.gov

Available to the public from the National Technical Information Service,  
U.S. Department of Commerce, 5285 Port Royal Rd., Springfield, VA 22161  
ph: (800) 553-6847  
fax: (703) 605-6900  
email: orders@ntis.fedworld.gov  
online ordering: <http://www.ntis.gov/ordering.htm>



This document was printed on recycled paper.

(9/2003)

**OFFICIAL USE ONLY**

# **Identify and Quantify the Mechanistic Sources of Sensor Performance Variation Between Individual Sensors SN1 and SN2**

## **M3AR-14PN2301022 Technical Letter Report**

AA Diaz

DL Baldwin

AD Cinson

AM Jones

MR Larche

RA Mathews

CA Mullen

AF Pardini

GJ Posakony

MS Prowant

TS Hartman

MK Edwards

July 2014

Prepared for  
the U.S. Department of Energy  
under Contract DE-AC05-76RL01830

Pacific Northwest National Laboratory  
Richland, Washington 99352



## Acknowledgments

The work reported here is a joint (collaborative) effort with Argonne National Laboratory (ANL), and was sponsored by the U.S. Department of Energy, Office of Nuclear Energy (NE), under U.S. Department of Energy Contract DE-AC05-76RL01830; Pacific Northwest National Laboratory (PNNL) Project No. 58745. Mr. Chris Grandy is the Technical Area Lead, and Mr. Bob Hill is the National Technical Director. Additionally, PNNL recognizes Mr. Tom Sowinski as the DOE Technical Manager and Mr. Carl Sink as the HQ Program Director.

PNNL would like to thank Mr. Grandy for his guidance and technical direction throughout the course of this effort. The Technical Team would also like to thank our colleagues at ANL for working jointly with PNNL staff over the course of this collaborative effort.

At PNNL, the authors wish to thank Ms. Katie Holton for her coordination and support of PNNL project logistics and for her help in handling travel-related reporting. The Team is indebted to Mr. Royce Mathews (also a co-author on this TLR) for providing in-Lab support across the entire spectrum of technical activities conducted on this project. In addition, the Team would like to express their thanks to Mr. Clyde Chamberlin, who was very responsive to our needs as we required his expertise in developing and employing an effective procedure for polishing the faceplate of the prototype probes, prior to in-sodium testing. The Team would also like to extend their gratitude to Ms. Lori Bisping for all of her hard work in providing administrative and financial reporting support to this project. Working with the PICS system can be challenging, and Lori's expertise and efficiency are second to none. Finally, the PNNL technical team would like to extend their thanks to Ms. Kay Hass for her ongoing support, attention to detail, and technical editing expertise in preparing and finalizing this Technical Letter Report.

PNNL is operated by Battelle for the U.S. Department of Energy under Contract DE-AC05-76RL01830.



## Acronyms and Abbreviations

ANL	Argonne National Laboratory
ASTM	American Society for Testing and Materials
dB	decibel
BW	bandwidth
DOE	U.S. Department of Energy
DOE-NE	U.S. Department of Energy, Office of Nuclear Energy
ETU	engineering test unit
FFT	fast Fourier transform
FY	fiscal year
ISI	inservice inspection
ISI&R	inservice inspection and repair
$\lambda$	wavelength
MARICO-2	Material Testing Rig with Temperature Control (version 2)
MHz	megahertz
NDE	nondestructive examination (or nondestructive evaluation)
Ni	nickel
PA	phased array
PA-UT	phased-array ultrasonic testing
PNNL	Pacific Northwest National Laboratory
rf	radio frequency
RT	radiographic testing
SFR	sodium-cooled fast reactor
SNR	signal-to-noise ratio
SN1	22-element array prototype serial number 1
SN2	22-element array prototype serial number 2
TLR	technical letter report
USV	under-sodium viewing
UT	ultrasonic testing



# Contents

Acknowledgments.....	iii
Acronyms and Abbreviations .....	v
1.0 Introduction .....	1.1
2.0 Objective and Scope .....	2.1
3.0 Key Performance Parameters .....	3.1
4.0 SN1 and SN2 Probe Design and Fabrication Differences .....	4.1
4.1 General 22-Element Array Design Considerations .....	4.1
4.1.1 SN1 and SN2 Mechanical Design.....	4.2
4.1.2 SN1 and SN2 Fabrication Process Differences (Enhancements) .....	4.2
5.0 Pre-Fabrication Evaluation of Individual PA-UT Probe Elements for SN1 and SN2 .....	5.1
6.0 Post-Fabrication Evaluation of Housed PA-UT Probes SN1 and SN2.....	6.1
6.1 Post-Fabrication Pulse-Echo Testing on Individual Array Elements (in Water) .....	6.1
6.1.1 Validation of Array Pin Connections .....	6.1
6.1.2 Evaluation of Transmit Uniformity per Element.....	6.3
6.1.3 Evaluation of Element-to-Element Cross-Talk .....	6.10
6.1.4 Evaluation of Selected Depth Focus Points .....	6.13
6.1.5 Evaluation of Selected Angles .....	6.15
6.2 Post-Fabrication Assessment of Temperature Resistance and Thermal Cycling Effects (in Hot Oil).....	6.16
6.3 Element-by-Element, Pulse-Echo, Ultrasonic Signal Responses for SN1 and SN2 Prototype Probes (in Water).....	6.18
6.3.1 Individual Element, Frequency Response Analysis, and Bandwidth Calculations for SN1 and SN2 Prototype Probes.....	6.19
6.4 Element-by-Element Sensitivity Analysis for SN1 and SN2 Prototype Probes.....	6.22
6.5 Sound Field Dimensional Characterization Analysis for SN1 and SN2 Prototype Probes.....	6.23
6.6 Spatial Resolution Analysis for SN1 and SN2 Prototype Probes.....	6.24
6.7 SNR Assessment for SN1 and SN2 Prototype Probes .....	6.27
7.0 Discussion and Conclusions .....	7.1
8.0 References .....	8.1

# Figures

2.1	Side-view Schematic, Illustrating the Japanese Joyo Reactor Fuel Sub-assembly and the Associated Cross-sectional Dimensions of an Isolated Pin, within the MARICO-2 Test Sub-assembly .....	2.2
4.1	Laser Machined Cup Assembly for the SN1 22-element Array and the SN2 22-element Array .....	4.2
4.2	Inspection of Nickel Faceplate-to-Piezoelectric Solder-bond Joint Integrity (SN1).....	4.3
4.3	High-frequency Acoustic Image for the Inspection of the Integrity of Nickel Faceplate-to-Piezoelectric Solder-bond joints of Two Different Element-cup Assemblies Fabricated in FY14.....	4.4
4.4.	Verification of Laser Machined Piezoelectric Against Critical-to-Performance Specifications .....	4.5
4.5	Close-up View of Elements and Channels of L4iS Laser-Machined Piezoelectric Wafer .....	4.5
4.6	Close-up View of a Corner on the Piezoelectric Wafer Showing Perimeter Laser Trimming .....	4.6
4.7	Insulated Copper Magnet Wires Soldered to the 22 Piezoelectric Elements of SN1 .....	4.7
4.8	Addition of High-Temperature Ceramic Adhesive/Epoxy Potting Material in SN1 .....	4.7
4.9	Addition of High-Temperature Ceramic Adhesive/Epoxy Potting Material in SN2 .....	4.8
4.10	SN1 Prototype Probe (left), and SN2 Prototype Probe (right).....	4.8
5.1	Pulse-echo Signal Response of a Single Element of the SN1 22-element PA Probe.....	5.2
5.2	Pulse-echo Signal Response of a Single Element of the SN2 22-element PA Probe.....	5.2
6.1	Line Scan of Element #15 for the SN1 Prototype Probe.....	6.2
6.2	Line Scan of Element #15 for the SN2 Prototype Probe.....	6.2
6.3	Raster Scan of Element #8 for the SN1 Prototype Probe.....	6.3
6.4	Raster Scan of Element #11, Showing a “Dead-Zone” Where no Ultrasonic Energy is Emitted .....	6.4
6.5	Raster Scan of Element #8 for the SN2 Prototype Probe.....	6.5
6.6	Raster Scan of Element #11 for the SN2 Prototype Probe.....	6.6
6.7	Raster Scan of All SN1 Elements Pulsed at 0-ns Delay.....	6.7
6.8	Raster Scan of All SN2 Elements Pulsed at 0-ns Delay.....	6.8
6.9	Cross-talk between Element #8 and Two Neighboring Elements for the SN1 Prototype Probe .....	6.11
6.10	Cross-talk between Element #8 and Two Neighboring Elements for the SN2 Prototype Probe .....	6.11
6.11	0° Depth Focus at 76.2 mm (3 in.) for the SN1 Prototype Probe.....	6.13
6.12	0° Depth Focus at 76.2 mm (3 in.) for the SN2 Prototype Probe.....	6.14
6.13	15° Azimuthal at a Depth Focus at 50.8 mm (2 in.) for the SN1 Prototype Probe .....	6.15
6.14	15° Azimuthal at a Depth Focus at 50.8 mm (2 in.) for the SN2 Prototype Probe .....	6.16
6.15	Photograph of the Laboratory Fume Hood Enclosure, Housing the Heating Plate/Oil Bath, the Prototype Probe, the Associated Manipulation Apparatus, and the Measurement Instrumentation .....	6.17

6.16	PA-UT Image Illustrating the 11-mm Pin and Backwall Signal Responses from Target #1 on the Bottom of the Hot-Oil Container at 260°C, Obtained from the SN2 Probe, and Monitored During Thermal Cycling and Resistance Tests .....	6.18
6.17	Photograph of the Laboratory Configuration for Capturing Ultrasonic Signal Responses for Assessing the Pulse-Echo Waveform Characteristics from a Standard Flat Target.....	6.19
6.18	Top: A-scan, rf Waveform of the First Arrival of the Ultrasonic Signal Response from the Fused Silica Reflector Block, for the SN1 Probe, Element #3. Bottom: The FFT of the Time-Gated Portion of the Waveform in the Top View. ....	6.20
6.19	Top: A-scan, rf Waveform of the First Arrival of the Ultrasonic Signal Response from the Fused Silica Reflector Block, for the SN2 Probe, Element #3. Bottom: The FFT of the Time-Gated Portion of the Waveform in the Top View. ....	6.20
6.20	Element-by-Element Sensitivity Variation between Both SN1 and SN2 Prototype Probes .....	6.23
6.21	Photograph of the Resolution Target Used to Assess Imaging Resolution Characteristics between SN1 and SN2 .....	6.24
6.22	PA-UT Image of the Resolution Target Using the SN1 Probe in Water at a Focal Distance of 76.2 mm (3.0 in.) .....	6.26
6.23	PA-UT Image of the Resolution Target Using the SN2 Probe in Water at a Focal Distance of 76.2 mm (3.0 in.) .....	6.26

## Tables

6.1	Dimensional Data Resulting from Face-Mapping of the SN1 Prototype Probe in Water.....	6.9
6.2	Dimensional Data Resulting from Face-Mapping of the SN2 Prototype Probe in Water.....	6.10
6.3	Results of Element-by-Element Cross-talk Measurements for the SN2 Prototype Probe .....	6.12
6.4	Passive and Active Sound Field Dimensions as a Function of the Focal Depth, at -6 dB Points, for both the SN1 and SN2 Prototype Probes.....	6.14
6.5	Element-by-Element Data and Calculations Resulting from the Frequency Response Analysis of Signal Responses from the SN1 and SN2 Prototype Probes, Captured from Immersion Testing in Water Using a Standard Reflector .....	6.21
6.6	Signal Response Data from a Quartz Reflector Block, for Assessment of Element-to-Element Sensitivity Between SN1 and SN2 Prototype Probes .....	6.22
6.7	True-State Dimensions of the Resolution Target Reflectors and Ultrasonically Measured Separation Dimensions from the PA-UT Data Obtained from SN1 and SN2 Probes.....	6.27



# 1.0 Introduction

This document is a Technical Letter Report (TLR) describing work conducted at the Pacific Northwest National Laboratory (PNNL) during FY 2014 on the under-sodium viewing (USV) project. This TLR satisfies the M3AR-14PN2301022 milestone, and is focused on identifying and quantifying the mechanistic sources of sensor performance variation between individual, 22-element, linear phased-array sensor prototypes, SN1 and SN2, respectively. The former prototype sensor was designed, fabricated, and tested in FY13 (with serial number 1) and the latter prototype sensor was designed, fabricated, and tested in FY14 (with serial number 2). This effort constitutes an iterative evolution that supports the longer term goal of producing and demonstrating a pre-manufacturing prototype ultrasonic probe that possesses the fundamental performance characteristics necessary to enable the development of a high-temperature sodium-cooled fast reactor (SFR) inspection system.

Sodium-cooled fast reactors are a technology of choice for advanced recycle reactors to be developed as part of the Gen IV Program. There is a need to re-establish the domestic technology infrastructure in order to support deployment of SFR technology. One key enabling technology is ultrasonic testing for under-sodium viewing that would be employed to (i) monitor operations in optically opaque sodium, and (ii) inspect structures, systems, and components within the reactor. PNNL's efforts are focused on demonstrating the use of linear phased-array ultrasonic probes to meet the needs of ranging and imaging in liquid SFRs. PNNL is currently developing linear phased-array ultrasonic testing (PA-UT) probes that are considered engineering test units (ETUs) that couple ultrasonic energy to the submerged structures of interest through liquid sodium. These probes provide the capability to image and conduct nondestructive examination (NDE) of critical components in high-temperature sodium-cooled fast reactors. The conceptual advantage of this approach is that the liquid sodium provides a medium that can directly couple the ultrasonic energy to the reactor components for imaging and inspection, if the liquid sodium is prepared, managed, and maintained appropriately (with regard to impurities and oxygen levels). The challenge is that the probe must withstand extended exposure to high temperatures and overcome wetting issues that can preclude the transmission of ultrasonic energy from coupling into the medium. PNNL demonstrated marginal success with the SN1 PA-UT probe in FY13, but the signal-to-noise ratio (SNR) was poor for in-sodium testing trials. The PNNL Technical Team anticipates improved results for in-sodium testing, based upon the pre- and post-fabrication assessments of the SN2 PA-UT probe in FY14. The aim of the FY14 work is to provide the technical justification for continuing the evolution of the performance capabilities and attributes of the SN2 PA-UT probe design, which is anticipated to be applicable to different inservice inspection (ISI) and repair procedures and/or component inspections as it matures.

Sodium-cooled fast reactors present some unique requirements in terms of technologies needed to support operations and maintenance. Inservice inspection and repair (ISI&R) methods must be developed to support deployment of advanced SFRs. Such reactors will require high plant availability (capacity factor) and long lifetimes, and will require advanced ISI&R technologies to ensure the integrity and safety of structures and components submerged in sodium, operating at elevated temperatures (~260°C). Key enabling technologies will allow operators to “see” through optically opaque sodium to support effective operations and maintenance activities. At the heart of the capability to image in sodium is the development of reliable probes to collect the basis data for reconstructing images of structures submerged in liquid sodium. This project is a joint Argonne National Laboratory (ANL) and PNNL project focused

on developing, demonstrating, and optimizing probe platforms capable of supporting anticipated ISI&R requirements. The baseline detection requirement, established during the first year (FY 2009) of the project, was derived from the need to detect a specific prototypic component (cross section of an isolated pin used within the MARICO-2 test subassembly). This benchmark has driven the prototype probe designs and performance evaluation methodologies. This report provides data, analyses, and the results of a comparative assessment of the performance characteristics of the two prototype, linear array ETUs, SN1 and SN2, respectively.

This TLR provides a technical summary of this effort, and in Section 2.0, the objectives and scope of the work are provided. Section 3.0 describes the key performance parameters that define the criteria for assessing probe characterization and performance attributes. Section 4.0 provides a summary of the design specifications and fabrication processes employed for development of the PA-UT probes. It also presents PNNL's initial modeling and simulation results associated with the design of the probes. Section 5.0 provides the results of pre-fabrication evaluations (prior to enclosure of the elements within the housings) of the SN1 and SN2 probe elements. Section 6.0 provides an assessment and discussion of the post-fabrication evaluations (after the elements were permanently mounted inside their respective housings) conducted on the SN1 and SN2 probes. This section includes results from both immersion water testing and immersion hot oil testing. Lastly, Section 7.0 provides the findings and discusses the comparative evaluation and conclusions from this work. References cited in this report are listed in Section 8.0.

## 2.0 Objective and Scope

An under-sodium viewing system will be an essential instrument for in-situ inspection of components of a sodium-cooled fast reactor. The USV system must be able to sustain operation in the high-temperature and corrosive environment of liquid sodium. At PNNL technical efforts are focusing on the development and demonstration of an effective and robust PA-UT imaging approach to address the inherent ISI challenges associated with imaging and resolving the specified MARICO-2 pin cross section within the Joyo reactor fuel sub-assembly geometry.

In FY10 through FY12, work at PNNL focused on identification and testing of commercially available phased-array probes; designing, fabricating, and testing single-element ultrasonic probes; designing a 24-element phased-array probe; and building/testing a 9-element phased-array probe that was successfully demonstrated in sodium at 260°C. In FY13, the PNNL Technical Team further refined design criteria using modeling and simulation tools and lessons learned from previous work, and subsequently developed methodologies for characterization of ETU linear phased-array probes, including:

- Radiographic testing (RT) – X-ray imaging and analysis
- Ultrasonic testing (UT) – Acoustic microscopy imaging and analysis
- Pre-fabrication assessments in water (after potting)
- Post-fabrication assessments (after housing the elements)
  - Immersion testing and characterization (in-water)
  - Immersion testing and characterization (in hot oil)
  - Immersion testing and characterization (in-sodium).

In addition, the Technical Team developed fixtures and specialized tooling to hold, position, and rotate the ETU probes under test. The 9-element linear PA-UT probe was fully characterized and shown to function and perform at a consistent level after 9 hours of immersion in-sodium. The design and assembly process was captured and documented for this 9-element probe, and used as a basis for the design, fabrication, and testing of a 22-element, linear PA-UT ETU. This probe (SN1) was assembled and tested in FY13 in-sodium up to the maximum temperature of 260°C; however, the majority of data were obtained at a constant temperature of 200°C, due to identified thermally induced performance limitations. The results of these tests indicated poor SNR in-sodium, which translated into marginal image quality and probe resolution, at best. The Team theorized possible root causes of the performance challenges and the analysis identified both thermo-mechanically induced issues coupled with poor sodium wetting. The former would be addressed with fabrication process enhancements, while the latter would be addressed with applying the appropriate level of sodium purification/regeneration, reduction of impurities and oxygen levels, and suitable probe faceplate polishing and surface conditioning to enhance wetting.

The objective of the work conducted at PNNL and reported here is to demonstrate the ability to detect a target feature, equivalent to the largest cross section of an isolated pin used within the MARICO-2 test sub-assembly, submersed in 260°C liquid sodium. Figure 2.1 illustrates the Japanese Joyo reactor fuel sub-assembly and the cross sectional dimensions of a simulated pin. In the present fiscal year (FY14),

emphasis is on completing the rebuild of the FY13 SN1 ETU PA-UT probe (with process enhancements), and testing this immersible linear array in water, hot oil (260°C), and eventually sodium, at temperature.

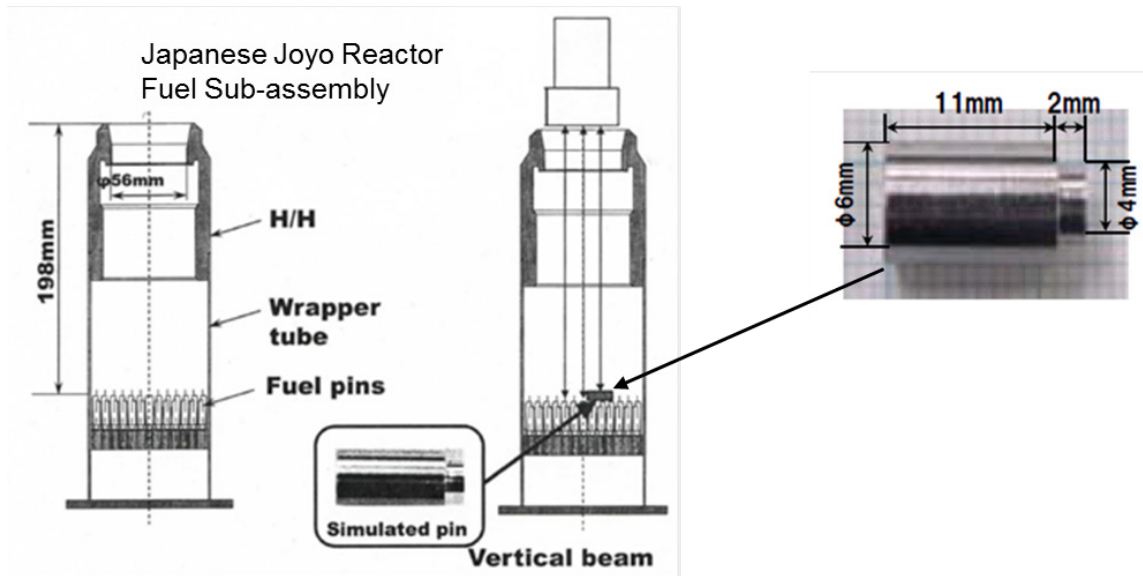


**Figure 2.1.** Side-view Schematic, Illustrating the Japanese Joyo Reactor Fuel Sub-assembly and the Associated Cross-sectional Dimensions of an Isolated Pin (simulated here), within the MARICO-2 Test Sub-assembly

The scope of the work for this portion of the PNNL effort conducted in FY14 includes performing a comparative evaluation and assessment of the performance characteristics of the SN1 and SN2 22-element PA-UT probes manufactured at PNNL. This assessment is based on probe performance in water and hot oil (at 260°C). In addition (and reported in a separate TLR), PNNL will assess and document the three-dimensional image quality resulting from in-sodium tests of the SN2 probe, as a function of primary inspection parameters. These include such variables as inspection time, spatial sampling frequency, sensor-to-target distance, sodium temperature, thermal cycling, etc. The work described here is based on technical evaluations and tests obtained at two different stages of fabrication: pre-fabrication – before the 22-element array was permanently enclosed within the sensor housing, and post-fabrication – after the 22-element array was permanently welded and enclosed within the housing.

### 3.0 Key Performance Parameters

This section of the report defines the key performance parameters and critical attributes that provide the criteria for assessing the performance, functionality, and effectiveness of a phased-array ultrasonic testing probe. The effort reported here is focused on analysis of data and performance metrics obtained from both PA-UT prototype probes, SN1 and SN2, respectively, to conduct a comparative assessment of the performance characteristics of these two ETU probes. In this report, the evaluation will not include performance of the probes in-sodium, but will instead focus on the performance characteristics via direct measurements obtained prior to housing the elements, after housing the elements, in water, and finally, in hot oil.

American Society for Testing and Materials (ASTM) E2491-13 is a standard guide for evaluating performance characteristics of phased-array ultrasonic probes (ASTM E2491-13). In addition, for PA-UT probes where single focal laws essentially fix the beam and electronic or sectorial scan modes are not employed, ASTM E1065 offers standard guidance using a ball target in an immersion test setting (ASTM E1065/E1065M-14). In FY13, PNNL reported some work in the Joint Technical Report on USV Progress with ANL that focused on obtaining data for characterization of the SN1 PA-UT probe (Braatz et al. 2013). The PNNL Technical Team used the key performance parameters outlined in this report, and also acquired data supporting the use of additional metrics and attributes for the prototype probes that were developed, to effectively compare performance of these ETUs. From the efforts conducted in FY13, the following characterization tests were conducted:

1. Pre-fabrication pulse-echo testing on individual array elements (in water)
2. Post-fabrication pulse-echo testing on individual array elements (in water)
  - a. Validation of array pin connections
  - b. Evaluation of transmit uniformity per element (using a pin-ducer as the receiving probe in raster scan mode)
  - c. Evaluation of element-to-element cross-talk (to assess inter-element coupling between neighboring elements)
  - d. Evaluation of selected depth focus points
  - e. Evaluation of selected angles (to assess how effectively the probe can skew the sound field off its 0° primary axis)
3. Post-fabrication assessment of temperature resistance and thermal cycling effects (in hot oil).

In addition to these tests, the PNNL Technical Team conducted post-fabrication characterization assessments aimed at quantifying a suite of additional critical attributes, including:

4. Individual voltage responses from each element after employing a standard excitation pulse, and reflected from a polished, fused silica reflector plate (conducted in pulse-echo mode, without the use of a separate pin-ducer for receiving signal responses)
5. Center and peak frequency responses from the FFTs of individual element responses in #4 above
6. -6 dB (decibels) bandwidths (BWs) of each element, calculated from #5 above

7. Sensitivity variations (in normalized % amplitude) from element-to-element
8. Sound field dimensions (focal spot size) at  $-6$  dB and  $-12$  dB points at a nominal distance from the face of the probe in water, using a pin-ducer receiving probe
9. Spatial resolution testing using raster scanning of the probe and employing flat reflectors with various spacings to evaluate array resolution performance in water
10. Evaluation of SNR from both pre-fabrication testing of the individual elements and post-fabrication tests.

With the analyses of data obtained from these performance characterization tests, the PNNL Technical Team was able to quantify key performance parameters that can be compared and contrasted between the two ETU probes, SN1 and SN2. In particular, sound field dimensions (spot size), resolution capabilities, SNR, frequency response, and BW characteristics constitute the suite of critical attributes used to evaluate these probes and to support any future decisions regarding viability for continued optimization in FY15. Examples of test data and results from these performance assessments are provided in Sections 5.0 and 6.0, and the conclusions obtained from a comparative evaluation of SN1 and SN2 probes are discussed in Section 7.0.

## 4.0 SN1 and SN2 Probe Design and Fabrication Differences

This section of the report summarizes the key design and fabrication aspects and differences between the SN1 and SN2 linear PA-UT probe designs, built at PNNL between FY13 and FY14, which to some degree, play a role in probe performance. Prior to embarking on the design of the first-generation 22-element PA-UT prototype probe (SN1), PNNL fully documented the 9-element probe design and fabrication methods/processes. The Team then developed a test methodology, test targets, and a probe positioner for characterizing next-generation PA prototypes by X-ray radiography, acoustic microscopy, and ultrasonic testing in water, hot oil, and in sodium. The 9-element probe was characterized and documented, and then the 22-element probe (SN1) was designed, fabricated, characterized, and tested in FY13. In FY14, the second-generation linear PA-UT probe (SN2) was developed. This design was similar to the design of the SN1 probe, but included modifications to the design and fabrication process protocols to accommodate lessons learned, improve SNR, and enhance overall probe performance.

As the project work unfolded in FY13, issues were identified relating to: (1) the bonding of the piezoelectric transducer multi-element crystal to the nickel (Ni) mounting substrate; (2) the laser machining of the phased-array element structures into the piezoelectric; (3) the reduced signal frequency of the 22-element phased array; (4) poor SNR; and (5) surface contour, thickness, and wetting issues (in-sodium). In FY14, the PNNL Technical Team focused on addressing these performance shortcomings with the SN1 probe by evaluating alternative methods, approaches, and processes associated with the design and fabrication stages for the SN2 probe. This included improvements and modifications to structural bonding processes, laser etching, soldering of the leads to the individual elements, ensuring a suitable bond of the multi-element crystal to the nickel substrate, improving surface polishing procedures, providing a thicker nickel faceplate, and enhancing sodium purification and regeneration processes to reduce impurities and oxygen levels in the sodium.

### 4.1 General 22-Element Array Design Considerations

For specific details associated with the entire SN1 probe design and fabrication process, the reader is directed to the FY 2012 and FY 2013 *Joint Technical Reports on Progress in Development of Ultrasonic Under-Sodium Viewing Technology to Enable Inspection Systems for In-Service Inspection and Repair of Liquid Metal Fast Reactors* (Watkins et al. 2012; Braatz et al. 2013). A simulation-based design study was conducted in FY13 to develop the SN1 ultrasonic linear array that would be compatible with PNNL imaging targets employed in the ANL sodium test facility. At that time, testing at ANL was planned as part of the FY13 scope for PNNL activities on this project. Therefore, the design of the SN1 probe incorporated required specifications to accommodate the facility requirements at ANL. The ANL facility uses a cylindrical sodium test tank with an inner diameter of 305 mm and height of 254 mm. The maximum sodium fill depth is 200 mm and the typical fill depth during sodium experiments is 150 mm. The array housing would be submerged approximately 25 mm below the sodium fill level and the array face would be pointed towards the bottom of the tank during data collection. The linear array images the target in a spherical coordinate system by electronically scanning along the polar axis as it rotates in azimuth. The 22-element SN1 linear array is an updated version of the 24-element design originally intended for use in the Joyo demonstration experiment. The element spacing was reduced by 25% so that the entire resolution target (designed at PNNL) could be imaged in a single scan within the constraints of

the ANL sodium test tank (Braatz et al. 2013). The array length is smaller because the required standoff distance for imaging is much shorter. The simulated ultrasonic performance of the 22-element array showed an expected spatial resolution along the array axis of approximately 2 mm in sodium. For the comparative assessment of the SN1 and SN2 probes provided in this TLR, spatial resolution in water will be determined and assessed, since in-sodium data have not yet been obtained for the SN2 probe.

#### 4.1.1 SN1 and SN2 Mechanical Design

From the 9-element prototype probe and for both SN1 and SN2 22-element arrays, the diameter of the nickel faceplate was increased to accommodate the need for a larger piezoelectric wafer (Watkins et al. 2012; Braatz et al. 2013). The number of coaxial cables and magnet wires increased from 9 to 22. Finally, the Swagelock VCR fitting was removed from the design. Other than these three changes, and the change of element pitch from 1.67 mm to 1.25 mm, there are no design differences between the 9-element and 22-element arrays.

#### 4.1.2 SN1 and SN2 Fabrication Process Differences (Enhancements)

The fabrication process outlined previously (in the FY12 and FY13 Joint TLRs) for the 9-element array was essentially followed for the SN1 and SN2 22-element arrays. However, some critical process improvements were introduced between the SN1 and SN2 design efforts. In particular, the bonding process for adhesion of the 22-element laser-machined crystal to the nickel faceplate was improved between SN1 and SN2 designs. Figure 4.1 shows the laser machined cup assembly for the SN1 probe (left) and the SN2 probe (right). Process improvements conducted by the vendor included improved solder materials, enhanced control of solder pooling, and employed a higher process temperature. As a result of this improved process, re-poling of the elements was not required for the SN2 probe, as it was for the SN1 probe.

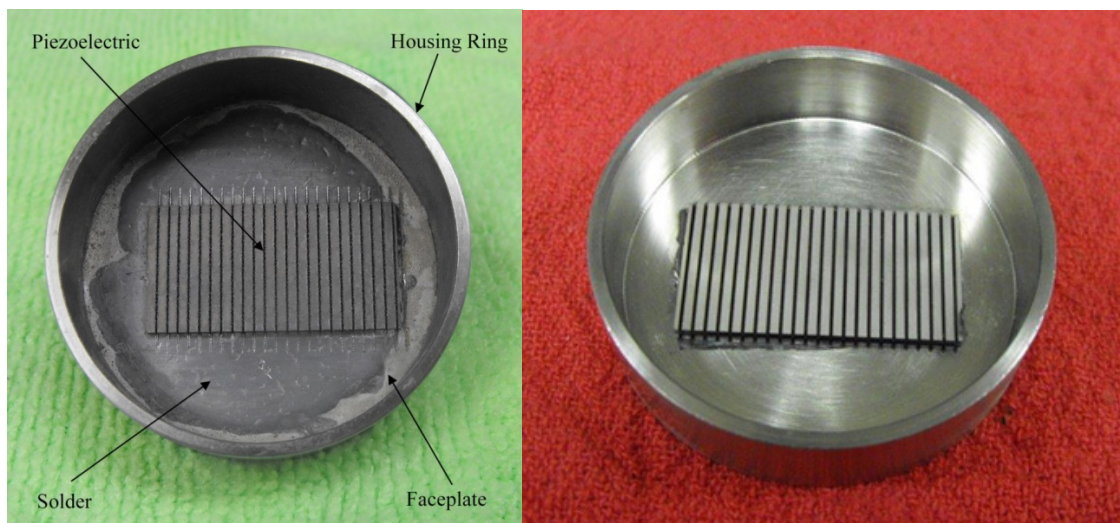


**Figure 4.1.** Laser Machined Cup Assembly for the SN1 22-element Array (left) and the SN2 22-element Array (right)

The SN1 piezo-element was soldered to the faceplate using a solder strip and hot plate procedure, where the Ni faceplate thickness was 0.062 in. The piezo-element faceplate was a separate structure and was welded to the element cup. The element was laser diced into 22 individual elements at 0.035-in. deep and 0.01-in. wide. The SN2 piezo-element was bonded to the cup assembly using a solder strip in an industrial oven at a temperature of 340°C, with a copper weight placed on top of the piezo-element to ensure even bonding between the element and the Ni faceplate. With the SN2 prototype, the Ni cup and faceplate were designed and fabricated as one assembly. The faceplate thickness increased to 0.100 in. and was then subsequently machined to 0.060 in. after completing the piezo-element solder/bonding process. The piezo-element was then laser diced to 0.035-in. deep and 0.01-in. wide. The SN2 piezo-element was then evaluated for any depoling of the piezo-element after the oven-baking process.

Figure 4.2 shows the result of inspecting the SN1 solder joint beneath the square piezoelectric element with acoustic microscopy (30 MHz) and by X-ray radiography. For acoustic microscopy, the bright white areas show where there is a dis-bond (void) in the solder joint between the piezoelectric and nickel faceplate. For radiography, the dark areas represent areas of dis-bond. The areas of dis-bond correlate well between the two inspection techniques. These dis-bond regions represent areas of high acoustic impedance and they have an undesirable impact on the final performance of the probe.

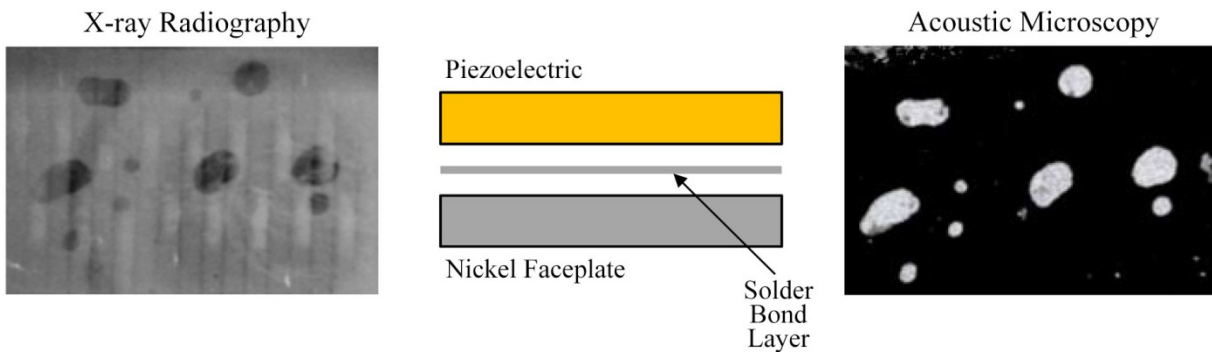


**Figure 4.2.** Inspection of Nickel Faceplate-to-Piezoelectric Solder-bond Joint Integrity (SN1)

Figure 4.3 shows the results of inspecting two different SN2 version solder joints, again using acoustic microscopy but at a slightly higher frequency (35 MHz). The bonding effectiveness and adhesion appears much more consistent than in the case of the SN1 prototype with the element shown on the right. This element was chosen for fabrication of the SN2 probe. Because good correlation was demonstrated between acoustic microscopy and X-ray imaging of the solder joint in FY13, X-ray imaging of these bonded structures was not conducted in FY14.

The sound field of the acoustic microscope was focused to insonify the inside surface of the nickel cup faceplate and the back surface of the piezo-element. These signals were gated in time and the assemblies were raster scanned. In this manner, properly soldered areas (that represent a strong bond) would allow the ultrasonic energy to penetrate through, while areas that were not soldered correctly would present a de-bonded area, essentially reflecting ultrasonic energy back to the focused probe. The acoustic imaging results are visually illustrated in Figure 4.3. Darker areas are associated with effective

soldering (sufficient bonding), while lighter areas indicate a lack of bonding because of ineffective soldering at a lower temperature. A temperature of 340°C was deemed optimal after evaluating multiple elements bonded to nickel faceplates in FY14.

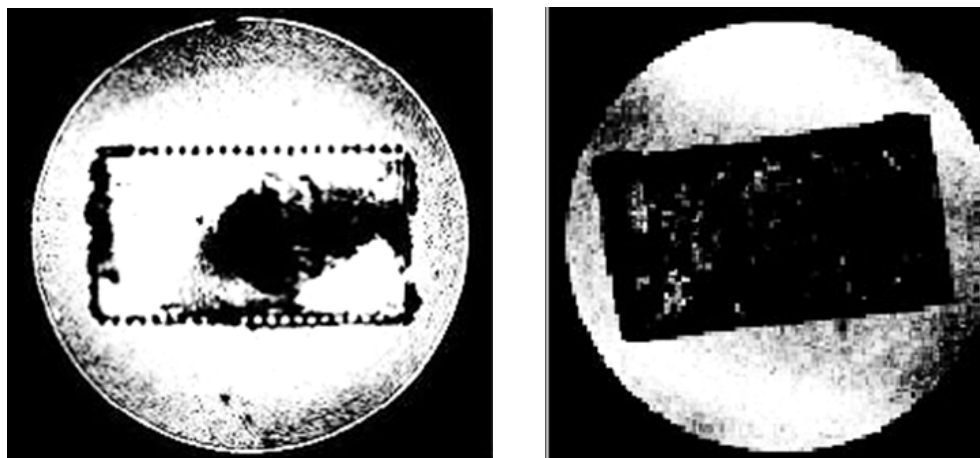


**Figure 4.3.** High-frequency Acoustic Image (35 MHz) for the Inspection of the Integrity of Nickel Faceplate-to-Piezoelectric Solder-bond joints of Two Different Element-cup Assemblies Fabricated in FY14. The element on the right was chosen for fabrication of the SN2 prototype probe.

In FY13, the SN1 piezoelectric element was laser machined by a vendor (Sigma Transducers, Inc., Richland, Washington) that manufactures ultrasonic transducers. Optical microscopy was used to inspect critical specifications of the machined material. Figure 4.4(a) shows a 110X magnification of the top surface of one element of the piezoelectric element. The width of this element (shown bounded by the red lines) was 1.002 mm against a specification of  $1 \pm 0.025$  mm. Figure 4.4(b) shows the typical channel gap between elements. The width of this channel gap (shown bounded by the red lines) was 0.249 mm against a specification of  $0.25 \pm 0.025$  mm. The laser machining process used produced relatively ragged edges, poorly defined channel geometries, and left residue in the channels that was manually removed. As these elements typically see 200V signals in operation, resistance tests were conducted to ensure there was electrical isolation element-to-element and element-to-ground (faceplate). In parallel with testing the SN1 22-element array, PNNL decided to pursue a more advanced laser machining process. In FY14 the laser engraving approach employed for the 9-element array and 22-element array SN1 revealed that there were a number of opportunities for improvement (Braatz et al. 2013). PNNL decided to pursue alternative piezoelectric machining approaches that would be capable of (1) producing cleaner, better cut elements, channels, and perimeter geometries; and (2) preserving the properties of the piezoelectric material (i.e., avoid depoling). Nominal design specifications for the dimensions of length and width for each individual element of both the SN1 and SN2 prototype probes was 15 mm (0.59 in.) by 1 mm (0.04 in.), respectively.

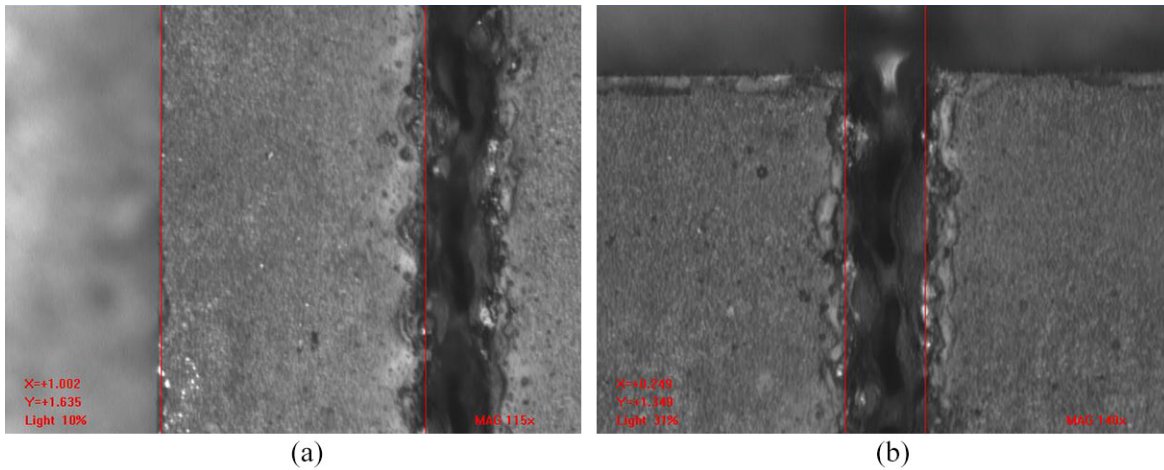


**Figure 4.4.** Verification of Laser Machined Piezoelectric Against Critical-to-Performance Specifications

Throughout FY14, PNNL pursued working with Lasers for Innovative Solutions, LLC (L4iS). This company had experience providing laser-machined piezoelectric material to phased-array probe manufacturing companies. They were able to produce three-dimensional precision-machined piezoelectric topographies without thermally compromising the material properties. The technique employs short-duration laser pulses during the machining process, which limits the heat-affected zone to a few microns. Figures 4.5 and 4.6 show close up views of the elements, channel geometries, and the perimeter. L4iS provided data to confirm element width and channel width dimensions met PNNL's specifications. By all standards, this new process exceeded the performance of the previously used laser engraving process (Sigma Transducers) and was successfully employed for the SN2 prototype probe.

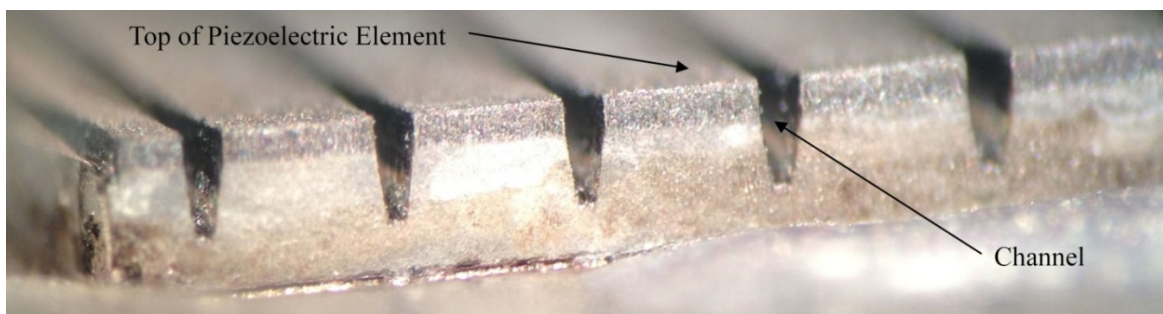


**Figure 4.5.** Close-up View of Elements and Channels of L4iS Laser-Machined Piezoelectric Wafer

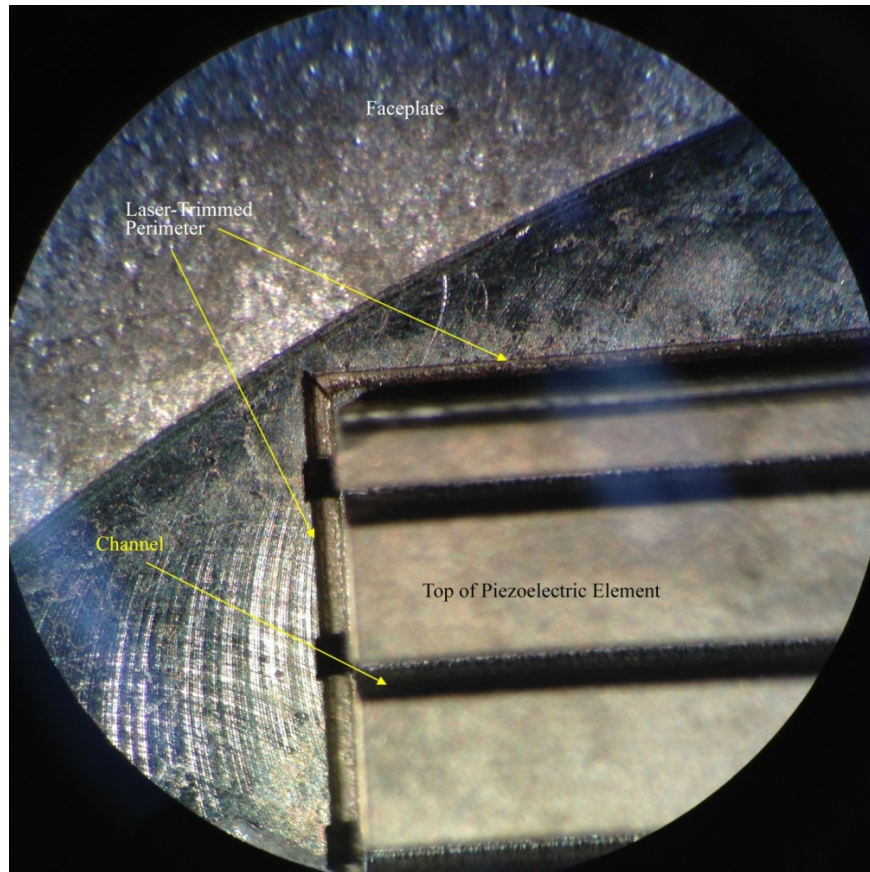


**Figure 4.6.** Close-up View of a Corner on the Piezoelectric Wafer Showing Perimeter Laser Trimming

For both SN1 and SN2 prototype designs, insulated magnet wire was soldered to each element. The processes employed for wiring, soldering, and backing the SN1 prototype probe are documented in great detail, in the FY13 Joint TLR (Braatz et al. 2013). Figure 4.7 shows the soldered assembly for the SN1 prototype probe. This soldering process was performed manually using a soldering iron. Not only are there opportunities for electrical shorts to occur, there is also the potential of locally overheating (exceeding 350°C) the piezo-element and causing the piezoelectric material to depole. The next step was to apply a high-temperature (1315°C) Resbond ceramic adhesive/epoxy potting material over the piezoelectric and magnet wires to a depth of ~7–8 mm as shown in Figure 4.8. This material serves as an acoustic backing to the piezoelectric elements and also as a strain relief for the magnet wires. This material controls the damping of the piezoelectric elements and also impacts the frequency response of the elements as well. In FY14, the soldering processes were improved, but the application process for the backing material was identical.



**Figure 4.7.** Insulated Copper Magnet Wires Soldered to the 22 Piezoelectric Elements of SN1

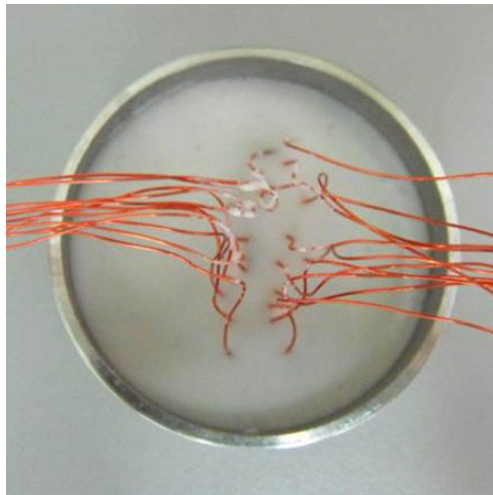


**Figure 4.8.** Addition of High-Temperature Ceramic Adhesive/Epoxy Potting Material in SN1

In FY14, refinements to the manual soldering technique were applied to the fabrication process of the SN2 probe. Instead of soldering all copper magnet wires in close proximity to each other near the middle of each element (as in the SN1 design), the wires were alternately soldered closer to the ends of the elements, providing additional spacing between wires and more effectively isolating each wire from the effects of adjacent electromagnetic conductivity between wires. Again, the high-temperature (1315°C) Resbond ceramic adhesive/epoxy potting material was applied over the piezoelectric and magnet wires to a depth of ~7–8 mm as shown in Figure 4.9.



**Figure 4.9.** Addition of High-Temperature Ceramic Adhesive/Epoxy Potting Material in SN2

The design and fabrication process differences described in this section underpin some significant performance improvements embodied in the SN2 prototype probe that will be discussed later, in Section 7.0 of this TLR. After housing had been completed, both probes appear identical from the outside as illustrated in Figure 4.10.

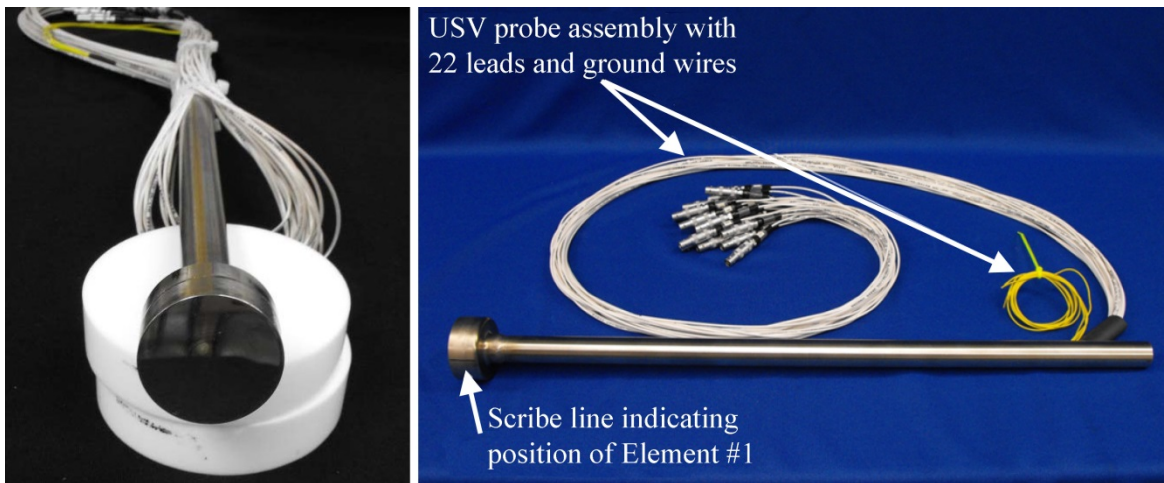


**Figure 4.10.** SN1 Prototype Probe (left), and SN2 Prototype Probe (right)

## 5.0 Pre-Fabrication Evaluation of Individual PA-UT Probe Elements for SN1 and SN2

This section describes the measurements and data obtained on the SN1 and SN2 prototype probes prior to housing the elements, but after potting of the laser etched, 22-element array within the Ni cup. A set of pulse-echo tests were conducted on the post-potted assemblies to (1) ensure that each individual array element provides an acoustic response to a narrow square-wave electrical input signal, (2) to make a relative comparison of the amplitude responses of each element to determine if any are “weak” or “unresponsive,” and (3) to establish a baseline for the amplitude response. Weak or unresponsive elements would be a qualitative indication of depoling occurring as a result of exceeding the piezoelectric Curie temperature of 350°C during the soldering processes. Depoling could be localized to a heat-affected zone in the vicinity of the magnet wire-to-piezoelectric solder joint, permitting the element to continue functioning, but with a weaker response. Unresponsive elements would indicate total depoling or alternatively an electrical disconnect of the magnet wire from the piezoelectric element. The tests were conducted by placing the external (sodium-facing side) of the cup assembly in a water bath spaced 1 cm away from a flat quartz crystal reflecting plate. Each individual element was driven with a short-duration 200V square-wave (80 ns) at a repetition rate of 3 kHz (UTEK Model UT 340 pulser/receiver). Pulse lengths shorter than 250 ns excite the piezoelectric at its fundamental design frequency 2 MHz and excite it at higher frequency modes of vibration. Ideally, an impulse function would be used, but an 80-ns pulse made it possible to achieve a sufficient signal amplitude response of long enough duration to make a meaningful assessment. Figure 5.1 shows the amplitude of the pulse-echo signal response of a single element versus time for the SN1 prototype probe.

The values of signal amplitude for the 22 elements ranged from 1–3 V (average 2V). The meaning of the absolute values of signal amplitude is not known, but they were recorded as a baseline for comparative purposes for future generation probes. Additionally, these signal responses provided approximate (and relative) indications of SNR values from element to element and probe to probe.

In Figure 5.2, a representative signal response from the SN2 22-element PA-probe is illustrated. The time-base is slightly different from that of the radio frequency (rf) waveform in Figure 5.1; however, the individual pulse-echo signal responses from the elements of the SN2 probe (with backing) resulted in signal responses that significantly reduced (dampened) the “ring down” providing a cleaner (less noisy) signal response.

From an analysis of these signal responses, it was clearly evident that the individual SNR values for the SN2 probe were substantially higher than those resulting from the SN1 probe in water, off of a quartz crystal reflecting plate. The SNR was generally 8–10 dB higher for the SN2 prototype array on an element-to-element basis. This corresponds to a voltage ratio enhancement of between 2.5-to-1 and 3.2-to-1 for the SN2 probe SNR over that of the SN1 probe.

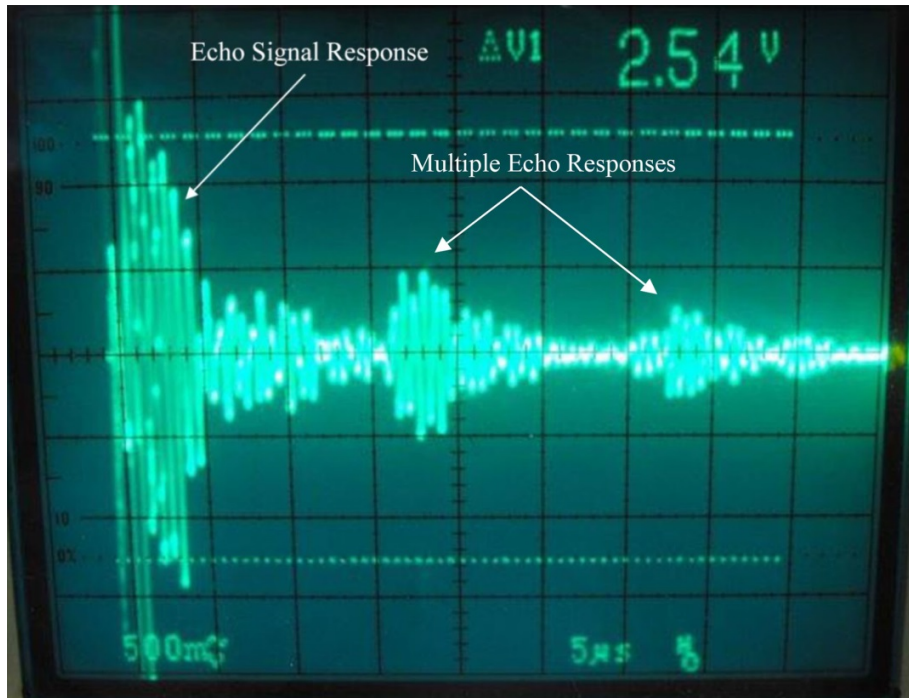


**Figure 5.1.** Pulse-echo Signal Response of a Single Element of the SN1 22-element PA Probe

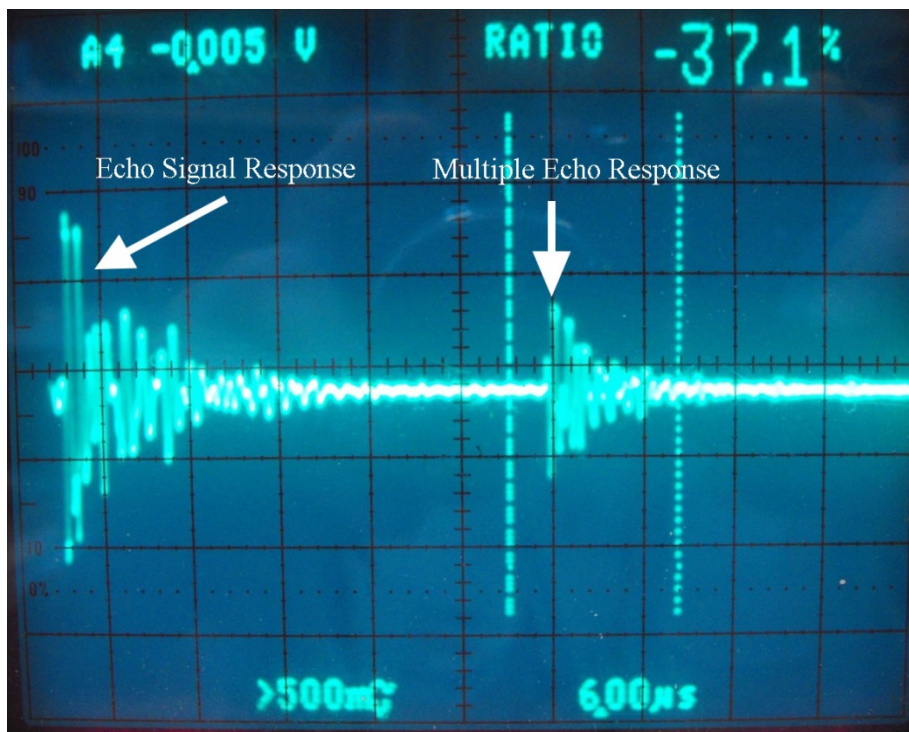


**Figure 5.2.** Pulse-echo Signal Response of a Single Element of the SN2 22-element PA Probe

## 6.0 Post-Fabrication Evaluation of Housed PA-UT Probes SN1 and SN2

This section describes the details of performance characterization assessments and functional testing for both the SN1 and SN2 22-element array prototype probes, after housing has been completed. This section includes the results of post-fabrication pulse-echo testing on individual array elements (in water), for validation of array pin connections; evaluation of transmit uniformity per element (using a pin-ducer as the receiving probe in raster scan mode); evaluation of element-to-element cross-talk (to assess inter-element coupling between neighboring elements); evaluation of selected depth focus points; and evaluation of selected angles (to assess how effectively the probe can skew the sound field off its 0° primary axis). In addition, this section provides a description of temperature resistance and thermal cycling effects (in hot oil) for both probes. Other critical attributes that are addressed in this section include individual voltage responses from each element after employing a standard excitation pulse, and reflected from a polished, fused silica reflector plate (conducted in pulse-echo mode, without the use of a separate pin-ducer for receiving signal responses). This test eliminates any effects introduced by the pin-ducer. The center and peak frequency responses from the FFTs of these individual element responses will also be computed and evaluated here. From this information, the -6 dB BWs of each element will be calculated and compared, and the sensitivity variations (in dB) from element-to-element will also be reported and discussed. The sound field dimensions (focal spot size) at -6 dB and -12 dB points at a nominal distance from the face of the probe in water, using a pin-ducer receiving probe, will be evaluated and contrasted. Results from spatial resolution testing using raster scanning of the probe (in pulse-echo mode) and employing elevated, flat reflectors with various spacings to evaluate array resolution performance in water, will be provided and assessed. Finally, an evaluation of SNR from both pre-fabrication testing of the individual elements and post-fabrication tests will be addressed.

### 6.1 Post-Fabrication Pulse-Echo Testing on Individual Array Elements (in Water)

This subsection describes post-fabrication, pulse-echo performance testing and functional validation on individual array elements (in water) for both the SN1 and SN2 probes.

#### 6.1.1 Validation of Array Pin Connections

Centering over the fiducial pin-ducer (0 point) with a standoff of 2 mm (0.8 in.), single line scans were executed along the primary axis of the array where only single elements were active (0-ns delay) during a given scan. The line scans were spatially encoded with a resolution of 0.25 mm (0.01 in.) for a scan length of 80 mm (3.1 in.). Each element was individually assessed for position location along the primary axis of the array and re-ordered at the Lemo connection point if necessary. Figure 6.1 shows the UltraVision reconstruction of the line scan of element #15 from the SN1 prototype probe. The line scan side view (left) is along the primary axis (blue axis) and the time-gated C-scan (top) view is on the right. The purple axis (in the left image) is the time or ultrasound axis. The response from element 15 is indicated by the red arrows in the figure. For reference, the fiducial pin-ducer response is circled in red and appears later in time. The purpose of the fiducial is to provide a physical spatial reference point. The positional information from each element was recorded such that the elements could be ordered in

ascending order of the linear array. All 22 elements were confirmed to be operational for both probes at the time these data were taken; however, some elements had significantly reduced activity. Figure 6.2 shows the same data for the same element (#15) for the SN2 prototype probe. Element #14 was found to be non-operational for the SN1 probe during the FY14 performance characterization tests.

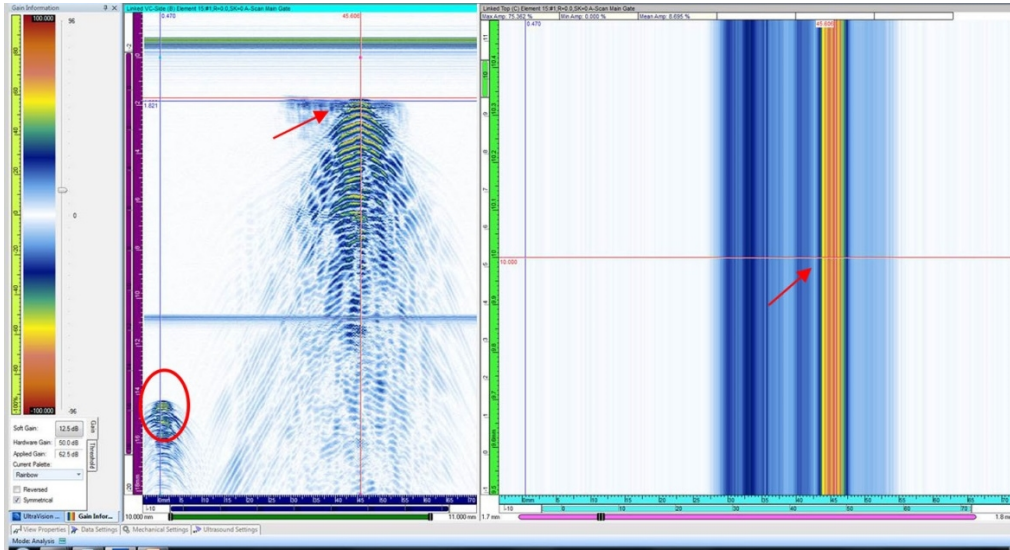


**Figure 6.1.** Line Scan of Element #15 for the SN1 Prototype Probe. Red arrows point to element 15 response; red circle indicates the fiducial response.

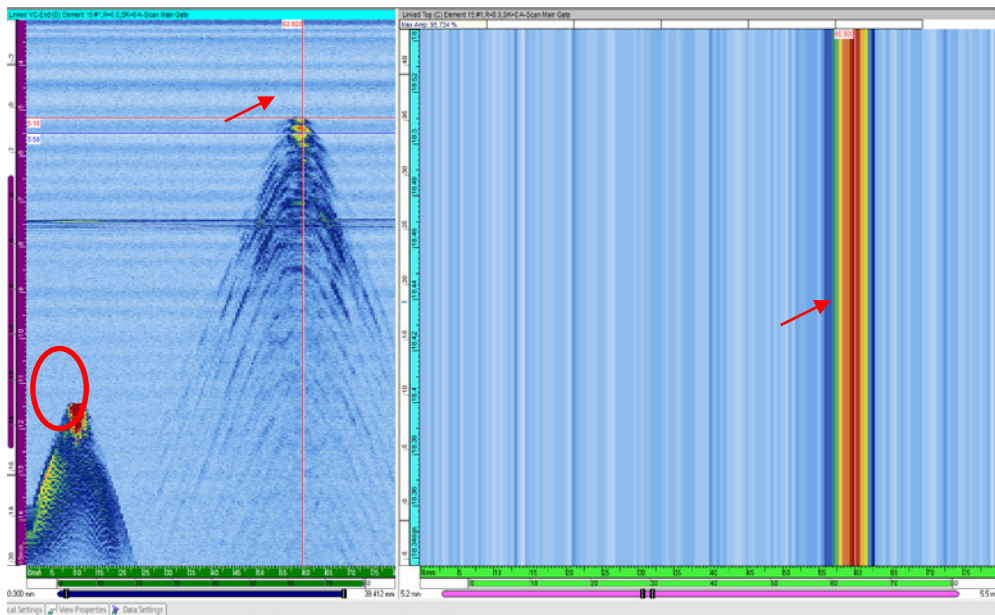


**Figure 6.2.** Line Scan of Element #15 for the SN2 Prototype Probe. Red arrows point to element 15 response; red circle indicates the fiducial response.

## 6.1.2 Evaluation of Transmit Uniformity per Element

Centering over the fiducial pin-ducer (0 point) with a standoff of 2 mm (0.8 in.), raster scans were executed beneath the face of the array where only single elements were active (0-ns delay) during a given scan. In addition, data were acquired with all elements active simultaneously with a 0-ns delay. The raster scans were spatially encoded with a resolution of 0.25 mm (0.01 in.) in the scan direction and for a scan length of 40 mm (1.6 in.) and 0.5-mm (0.02-in.) resolution in the index axis for a length of 75 mm (2.95 in.). Each element was imaged both individually as well as in concert. Figure 6.3 shows the UltraVision reconstruction of the raster scan of element #8 (as an example) from the SN1 prototype probe using cutoff for the dynamic range. The raster scan side view (left) is along the primary axis (blue axis) and the time-gated C-scan (top) view is on the right. The purple axis (in the left image) is the time or ultrasound axis. The response from element 8 is indicated by the red arrows in the figure. Here it is shown that the element length in the passive axis is approximately 16 mm (0.63 in.) corresponding well with the 15-mm physical length of the as-built element. Similarly, element #11 (from the SN1 prototype probe) is shown in Figure 6.4, also using no dynamic range cutoff. Element #11 is an example that illustrates a reduced passive aperture or “dead-zone” where no ultrasonic energy is being emitted (highlighted by the red box). This would most likely be caused by a void in the solder interface between the nickel faceplate and the piezoelectric wafer. The acoustic microscopy and radiographic images taken of this joint during fabrication did reveal the existence of voids in the solder joint. An overlay of voids and element dead-zones would confirm this. Red arrows identify the primary element being evaluated.

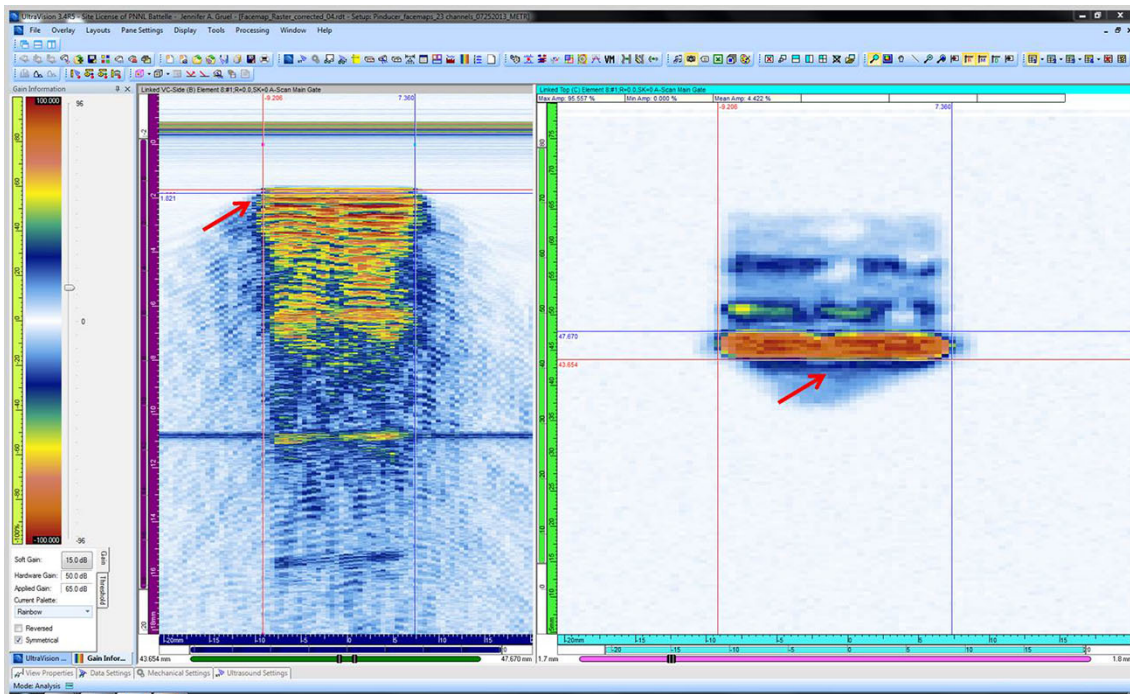
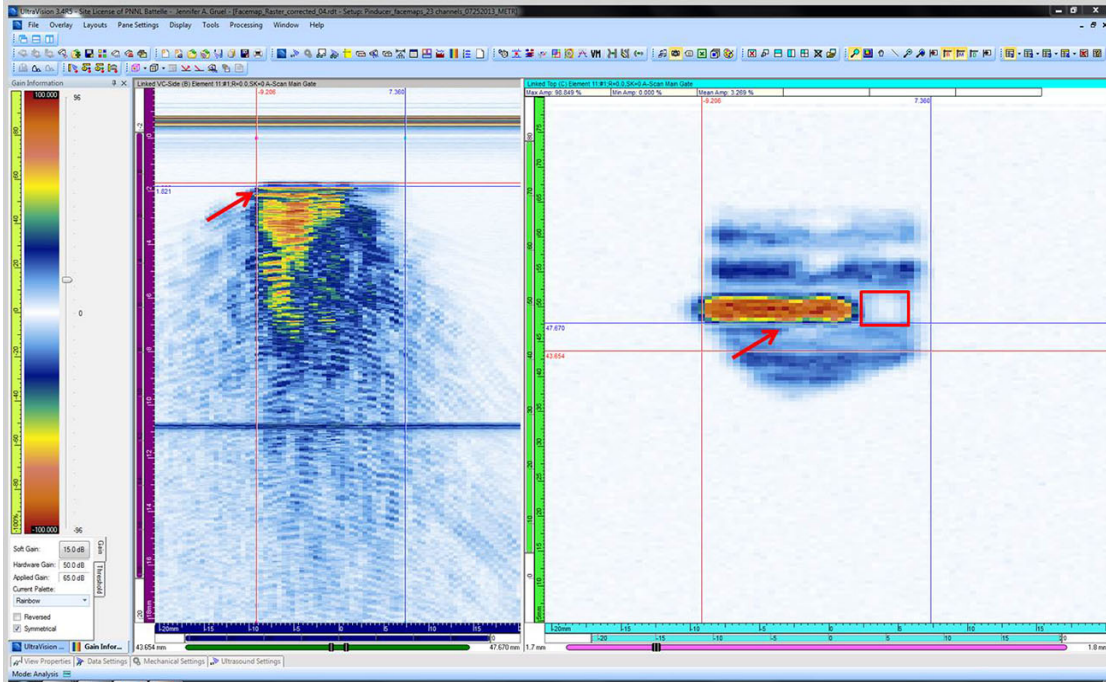
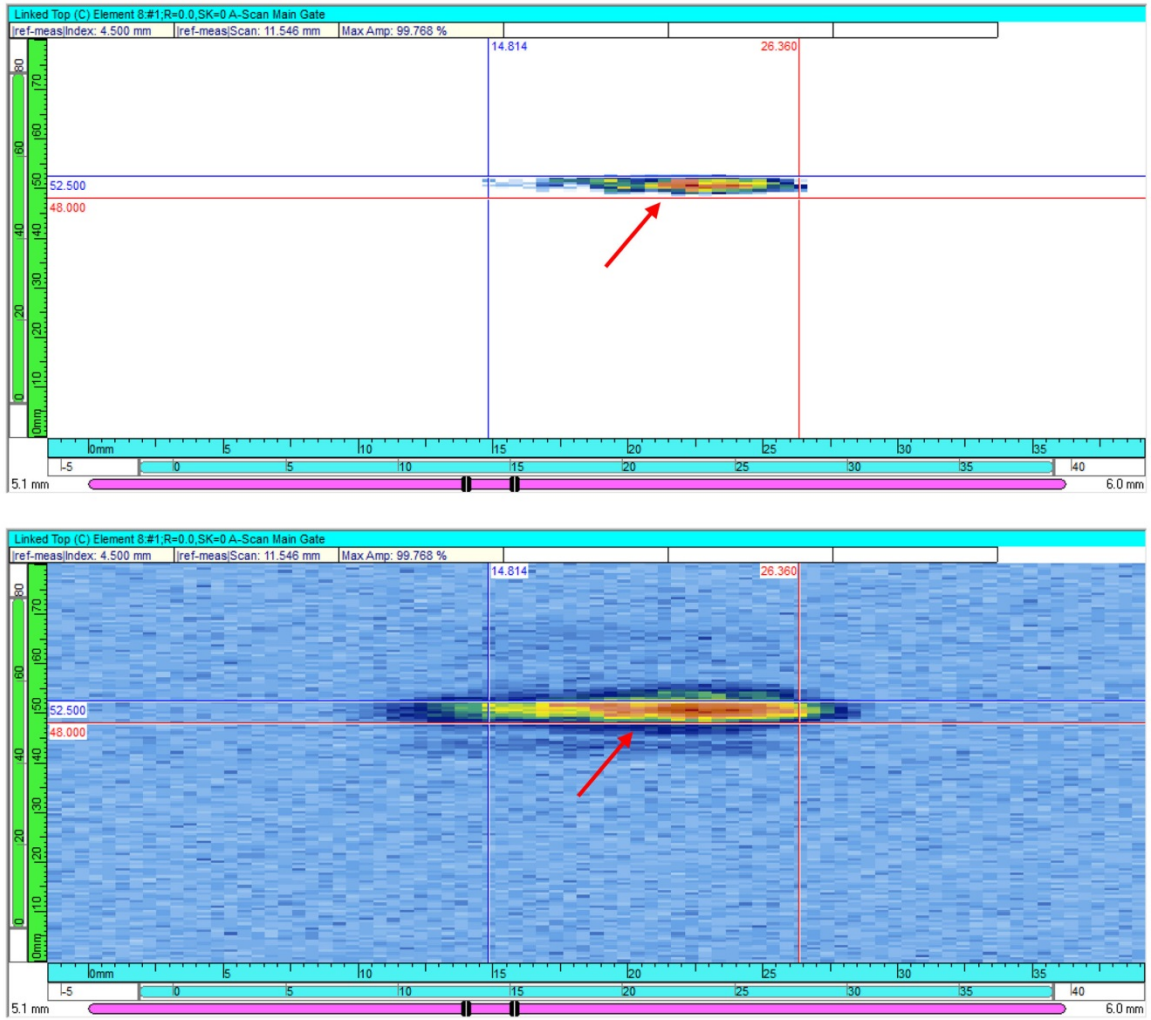


Figure 6.3. Raster Scan of Element #8 for the SN1 Prototype Probe



**Figure 6.4.** Raster Scan of Element #11 (for the SN1 prototype probe), Showing a “Dead-Zone” Where no Ultrasonic Energy is Emitted (indicated by the area within the red box)

Figures 6.5 and 6.6 provide the same ultrasonic images for the same elements from the SN2 prototype probe, but both the  $-6$  dB cutoff and the full dynamic range images are provided for each scenario. Figure 6.5 provides the raster scan data from element #8, while Figure 6.6 provides the raster scan data for element #11. Again, in similar fashion from the assessment of the SN1 probe, the response from element #8 is indicated by the red arrows in the figures. This time, for the SN2 views, we have eliminated the side view image provided in Figures 6.3 and 6.4.



**Figure 6.5.** Raster Scan of Element #8 for the SN2 Prototype Probe. Top:  $-6$  dB cutoff C-scan view; Bottom: full dynamic range C-scan view, with no cutoff.

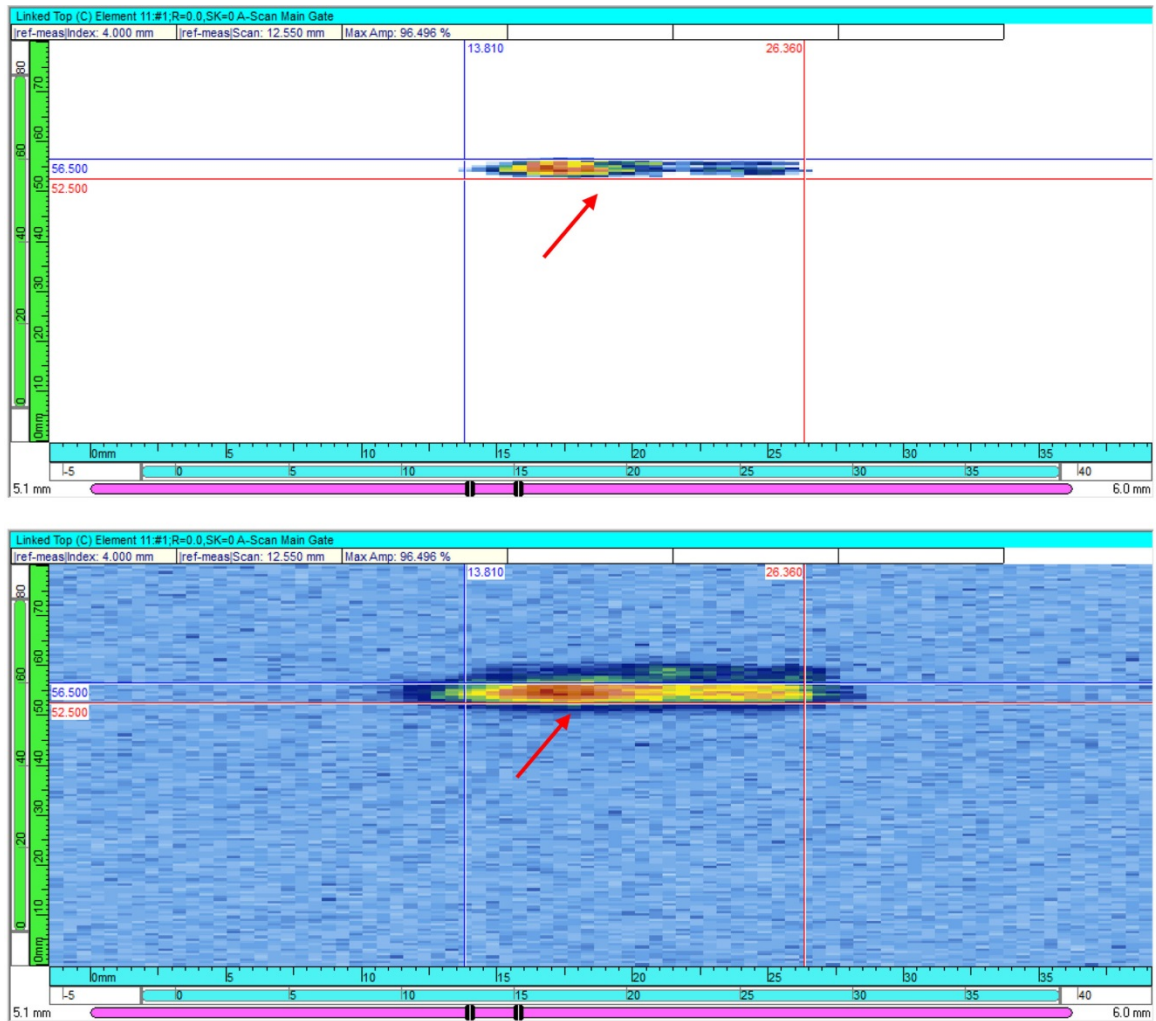


**Figure 6.6.** Raster Scan of Element #11 for the SN2 Prototype Probe. Top:  $-6$  dB cutoff C-scan view; Bottom: full dynamic range C-scan view, with no cutoff.

Here, for element #8 of the SN2 probe, it is shown that the element length in the passive axis is approximately 11.6 mm (0.45 in.) at  $-6$  dB, and 16.6 mm (0.65 in.) at the  $-12$  dB points, corresponding well with the 15-mm physical length of the as-built element. For element #11 of the SN2 probe, again, the  $-6$  dB and  $-12$  dB dimensions for the element passive lengths are very similar to the dimensions for element #8, indicating a more consistent excitation and utilization of the elements (acoustically). No dead zones were identified in this evaluation for the SN2 probe; however, there were zones identified on some elements that were transmitting less energy than other areas of the same element.

Overall, sufficient activity of all elements of the SN1 probe is shown in Figure 6.7. Here, all of the elements of the SN1 array are pulsing simultaneously (with a delay of 0 ns between them) and the pinducer is raster scanned over the entire aperture of the array. It is noticed that there are two regions of inactivity near the first few elements of the array (i.e., elements 1–5). The lack-of-activity regions are highlighted by white dashed triangles in the image on the right. It is believed that these areas of inactivity

most likely correspond to dis-bond in the solder joint between the nickel faceplate and the piezoelectric, but this will need to be confirmed by a physical autopsy of the probe. The acoustic microscopy and radiographic images taken of this joint during fabrication did not reveal the presence of dis-bond occurring immediately after soldering.

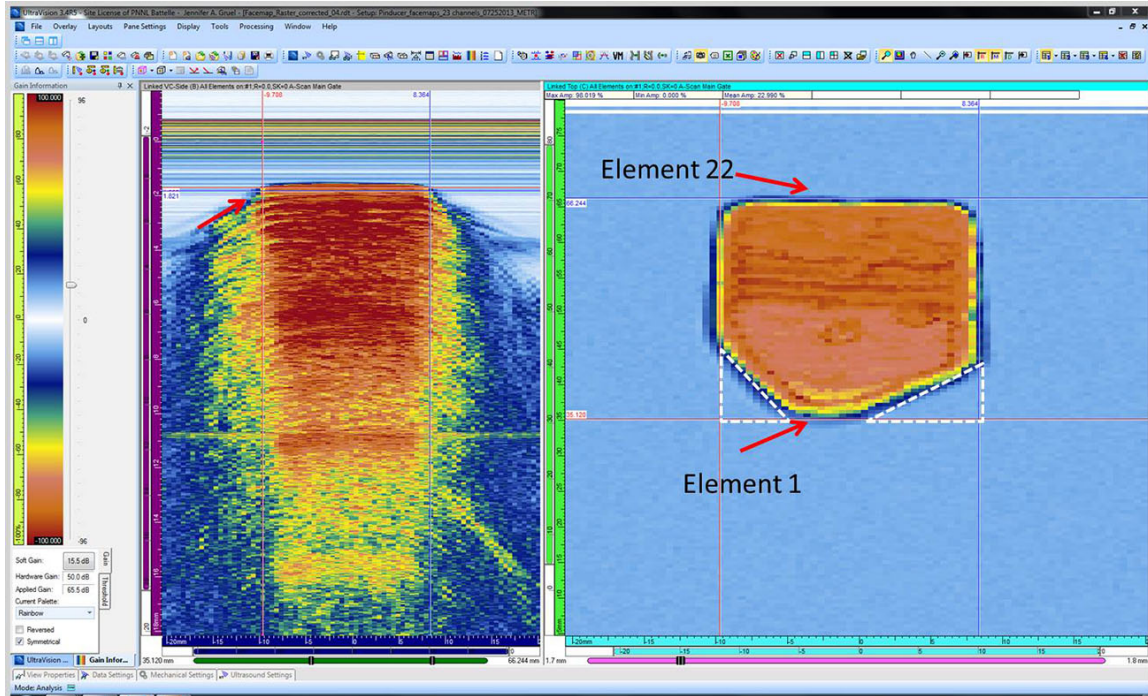


**Figure 6.7.** Raster Scan of All SN1 Elements Pulsed at 0-ns Delay. Red arrows indicate active aperture of array.

It was noted at this stage of testing that although the SN1 array was pulsed using a 250-ns square-wave excitation corresponding to 2 MHz, the received frequency response from each element centered at approximately 1.07 MHz after performing fast Fourier transforms on the time-amplitude A-scan data.

Again, in similar fashion to the evaluation of the SN1 probe, the overall activity of all elements of the SN2 probe is shown in Figure 6.8. While there is no evidence of dis-bonding over the aperture of the SN2 array, it is noted that there are elements that emit more acoustic energy than others across the 22 elements of the array. In addition, we omitted the side view in Figure 6.8 and instead included both the  $-6$  dB face map as well as the full dynamic range (no amplitude clip) C-scan images for the SN2 prototype probe.

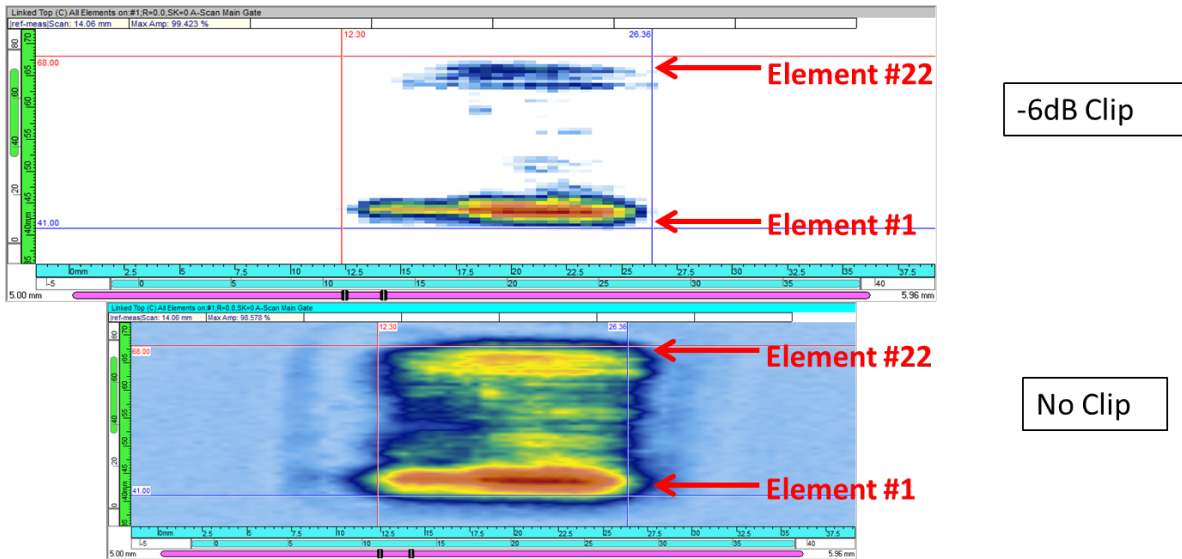


**Figure 6.8.** Raster Scan of All SN2 Elements Pulsed at 0-ns Delay. Red arrows indicate active aperture of array. Figure 6.7 compares directly to the “no-clip” C-scan image on the bottom.

Exciting all elements of the array with no delays allows the probes to be treated as a single-element conventional array. While doing this, a pin-ducer was rastered under the array to map the signal responses and essentially capture hot/cold spots of the array in the X-Y plane under the probe at a specified distance from the probe face in water. The data for the SN2 probe show that the first and last few elements have higher amplitudes than most of the other elements in the array.

Tables 6.1 and 6.2 provide the measured lengths and widths of the individual elements for both SN1 and SN2 probes, respectively, at both  $-6$  dB and  $-12$  dB points of the sound field maps. It should be noted that this exercise was not conducted to obtain accurate dimensions of the individual elements, but was aimed at evaluating the degree of spatial uniformity associated with effective excitation of each individual element. Because of divergence of the sound energy while pulsing the elements with no delays, the measured dimensions provided in these tables will indicate areas that are not being excited appropriately, or areas where dis-bonding has occurred, precluding the element from coupling energy out of the probe. But these data should not be used to accurately measure the individual element dimensions. For Tables 6.1 and 6.2, the length values correspond to the passive X axis of the probe and the width values correspond to the active Y axis of the probe. For the SN1 prototype probe, the  $-6$  dB average length and width is 13.9 mm (0.55 in.) by 3.38 mm (0.13 in.). The  $-12$  dB average length and width is 14.88 mm (0.59 in.) by 4.45 mm (0.18 in.). For the SN2 prototype probe, the  $-6$  dB average length and width is 12.28 mm (0.48 in.) by 4.41 mm (0.17 in.). The  $-12$  dB average length and width is 16.04 mm (0.63 in.) by 7.93 mm (0.31 in.). These values can be loosely compared to the actual individual element dimensions (based on specifications provided in the FY13 TLR) of 15 mm (0.59 in.) length by 1.0 mm (0.04 in.) width for both the SN1 and SN2 prototype probes.

**Table 6.1.** Dimensional Data Resulting from Face-Mapping of the SN1 Prototype Probe in Water

Element #	-6 dB				-12 dB			
	Length (Passive X)		Width (Active Y)		Length (Passive X)		Width (Active Y)	
	(mm)	(in.)	(mm)	(in.)	(mm)	(in.)	(mm)	(in.)
1	7.53	0.30	5.52	0.22	9.54	0.38	7.53	0.30
2	8.53	0.34	5.02	0.20	10.04	0.40	6.53	0.26
3	8.03	0.32	3.51	0.14	9.54	0.38	4.52	0.18
4	10.04	0.40	4.52	0.18	11.55	0.45	5.52	0.22
5	13.05	0.51	2.51	0.10	14.06	0.55	3.51	0.14
6	14.56	0.57	3.01	0.12	15.56	0.61	5.02	0.20
7	15.06	0.59	3.51	0.14	16.06	0.63	4.52	0.18
8	15.56	0.61	3.51	0.14	16.57	0.65	4.52	0.18
9	16.06	0.63	3.51	0.14	17.07	0.67	4.02	0.16
10	16.06	0.63	3.51	0.14	17.07	0.67	4.52	0.18
11	10.54	0.42	2.51	0.10	11.04	0.43	3.51	0.14
12	16.06	0.63	3.01	0.12	16.06	0.63	3.51	0.14
13	15.06	0.59	2.01	0.08	15.06	0.59	2.51	0.10
14	15.56	0.61	3.01	0.12	16.57	0.65	4.02	0.16
15	15.56	0.61	2.51	0.10	16.57	0.65	4.52	0.18
16	15.56	0.61	3.01	0.12	16.57	0.65	4.02	0.16
17	15.56	0.61	3.51	0.14	16.57	0.65	3.51	0.14
18	15.56	0.61	3.01	0.12	16.57	0.65	4.52	0.18
19	15.56	0.61	3.51	0.14	16.06	0.63	4.52	0.18
20	15.56	0.61	3.51	0.14	16.06	0.63	4.52	0.18
21	15.06	0.59	3.01	0.12	16.06	0.63	4.02	0.16
22	15.56	0.61	3.51	0.14	17.07	0.67	4.52	0.18
<b>Average</b>	13.90	0.55	3.38	0.13	14.88	0.59	4.45	0.18
<b>Standard Deviation</b>	2.81	0.11	0.79	0.03	2.58	0.10	1.03	0.04

**Table 6.2.** Dimensional Data Resulting from Face-Mapping of the SN2 Prototype Probe in Water

Element #	-6 dB				-12 dB			
	Length (Passive X)		Width (Active Y)		Length (Passive X)		Width (Active Y)	
	(mm)	(in.)	(mm)	(in.)	(mm)	(in.)	(mm)	(in.)
1	13.55	0.53	5.50	0.22	16.57	0.65	8.00	0.31
2	13.55	0.53	5.50	0.22	17.57	0.69	8.50	0.33
3	13.55	0.53	6.00	0.24	16.06	0.63	9.00	0.35
4	13.55	0.53	6.00	0.24	16.57	0.65	9.00	0.35
5	14.06	0.55	6.00	0.24	17.07	0.67	10.00	0.39
6	14.06	0.55	4.50	0.18	16.06	0.63	8.50	0.33
7	15.06	0.59	6.00	0.24	18.57	0.73	10.00	0.39
8	11.55	0.45	4.50	0.18	16.57	0.65	8.50	0.33
9	14.06	0.55	3.50	0.14	15.06	0.59	6.50	0.26
10	6.53	0.26	3.00	0.12	14.06	0.55	7.00	0.28
11	12.55	0.49	4.00	0.16	16.06	0.63	9.00	0.35
12	7.53	0.30	3.50	0.14	14.56	0.57	6.50	0.26
13	13.05	0.51	3.50	0.14	15.06	0.59	6.50	0.26
14	9.04	0.36	5.00	0.20	15.56	0.61	9.50	0.37
15	13.55	0.53	3.50	0.14	15.56	0.61	5.50	0.22
16	8.03	0.32	3.50	0.14	15.06	0.59	6.50	0.26
17	12.55	0.49	4.00	0.16	17.07	0.67	7.00	0.28
18	13.05	0.51	3.00	0.12	16.06	0.63	6.00	0.24
19	13.05	0.51	4.00	0.16	16.06	0.63	7.50	0.30
20	13.05	0.51	4.00	0.16	15.56	0.61	8.00	0.31
21	12.55	0.49	4.00	0.16	15.56	0.61	9.00	0.35
22	12.55	0.49	4.50	0.18	16.57	0.65	8.50	0.33
<b>Average</b>	12.28	0.48	4.41	0.17	16.04	0.63	7.93	0.31
<b>Standard Deviation</b>	2.26	0.09	1.00	0.04	1.00	0.04	1.29	0.05

### 6.1.3 Evaluation of Element-to-Element Cross-Talk

A separate analysis performed on data acquired from both SN1 and SN2 probes indicated the amount of signal leakage from element to element. The individual element raster scans captured energies received from neighboring elements and showed that energy was either mechanically transferred or individual elements were electrically connected within the array. This measure of element isolation revealed that on average the element-to-element cross-talk for the SN1 prototype probe was on the order of -7 dB, while the SN2 prototype probe resulted in an improved element-to-element cross-talk range of approximately -13 dB. The 6 dB difference essentially equates to a factor of 2 improvement in cross-talk reduction. Figures 6.9 and 6.10 show examples of cross-talk between neighboring array elements when only element #8 is pulsed (as examples) for both the SN1 and SN2 prototype probes, respectively. The low level of isolation for the SN1 array was a surprising outcome. In FY13, the 9-element array achieved -32 dB of isolation (with -30 to -35 dB being ideal) (Braatz et al. 2013). One possible contributing factor to the reduction in isolation was considered to be coupling between the insulated but bundled magnet wires that are soldered to the back of the individual piezoelectric elements. An electromagnetic

analysis (ANSYS – HFSS) was performed that simulated the conditions of the cross-talk test. The result was that the electromagnetic fields and current densities induced by one activated magnet wire running nearby and parallel to another magnet wire resulted in approximately  $-30$  dB isolation between elements.

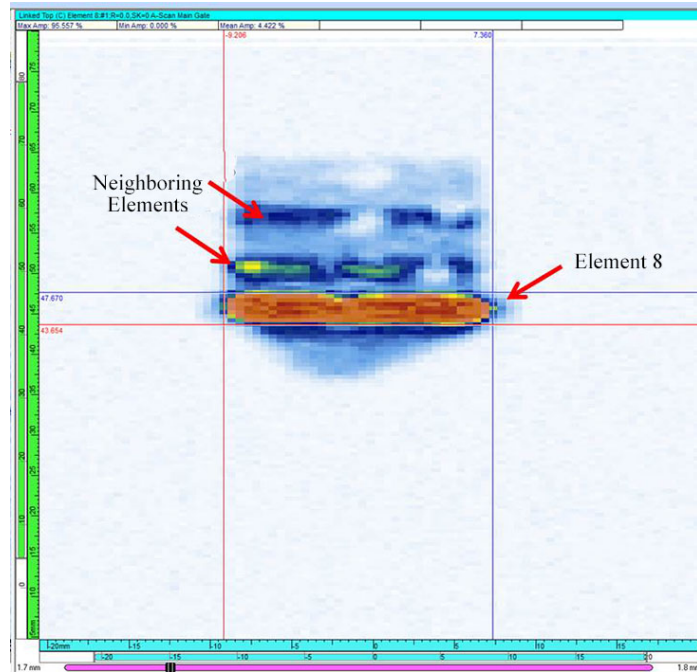


**Figure 6.9.** Cross-talk between Element #8 and Two Neighboring Elements for the SN1 Prototype Probe

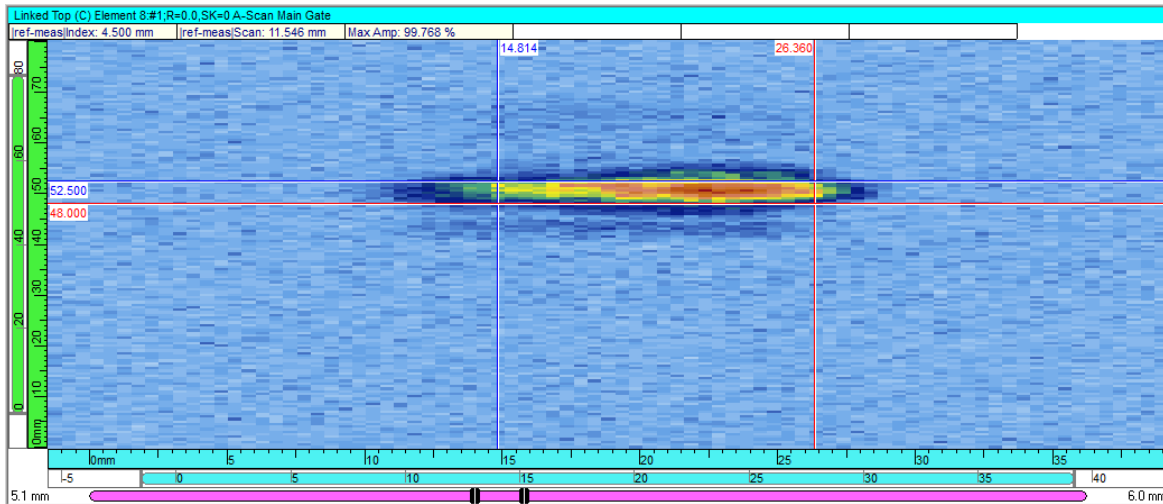


**Figure 6.10.** Cross-talk between Element #8 and Two Neighboring Elements for the SN2 Prototype Probe

The impact this low level of isolation has on the SN1 array performance is unknown and will need to be investigated in the future. One likely possible contributing factor is the reduced spacing between elements of the 22-element array as compared with that of the 9-element array. The element-to-element cross-talk was more effectively isolated for the SN2 probe, but there is room for more improvement here. The enhanced cross-talk values for the SN2 probe may be attributed to a combination of factors, including the improved laser dicing process, the alternate spacing used for soldering magnet wires on each element, and improved damping of the piezo-element. While the cross-talk values (in dB) for the SN1 prototype probe were reported in the FY13 TLR, the values for the SN2 prototype probe can be found in Table 6.3.

**Table 6.3.** Results of Element-by-Element Cross-talk Measurements for the SN2 Prototype Probe

<b>Element#</b>	<b>Soft Gain (dB)</b>	<b>Element Max Amp (%)</b>	<b>Noise Mean (%)</b>	<b>Cross-talk Region Max Amp (%)</b>	<b>Element Isolation (dB)</b>	<b>SNR (dB)</b>
1	28.0	95.669	8.08	22.07	-12.74	-21.47
2	28.5	98.74	10.75	28.58	-10.77	-19.26
3	28.5	94.842	8.24	20.79	-13.18	-21.22
4	29.0	99.084	10.95	30.27	-10.30	-19.13
5	31.5	97.266	11.88	29.36	-10.40	-18.27
6	31.0	95.285	10.65	22.52	-12.53	-19.04
7	33.5	94.72	13.88	32.34	-9.33	-16.68
8	30.5	99.768	12.27	26.17	-11.62	-18.20
9	26.5	97.003	6.58	15.48	-15.94	-23.38
10	28.0	94.44	6.65	14.72	-16.15	-23.04
11	30.5	96.496	10.71	24.53	-11.89	-19.10
12	27.5	98.419	7.06	13.90	-17.00	-22.88
13	30.5	98.135	9.85	21.26	-13.28	-19.97
14	30.5	98.132	10.31	19.63	-13.98	-19.57
15	30.0	95.734	10.18	21.62	-12.93	-19.47
16	29.0	97.705	8.31	31.65	-9.79	-21.41
17	30.5	99.768	11.65	22.90	-12.78	-18.66
18	27.0	98.379	7.84	14.21	-16.81	-21.98
19	29.5	96.207	9.06	20.41	-13.47	-20.53
20	29.5	96.207	9.85	20.41	-13.47	-19.79
21	29.5	96.207	9.74	21.86	-12.87	-19.89
22	30.5	99.768	11.37	21.26	-13.43	-18.86
<b>Average</b>					-12.94	-20.08
<b>Standard Deviation</b>					2.10	1.73

### 6.1.4 Evaluation of Selected Depth Focus Points

While the modeled working distance for the 22-element array was up to 154 mm (6.06 in.), depth focusing capabilities were imaged at standoff distances of 25.4, 50.8, and 76.2 mm (1.0, 2.0, and 3.0 in.) because of the practical nature of these depths in sodium. Attempts to focus the sound field effectively at depths greater than 76.2 mm (3.0 in.) in sodium with SN1 were unsuccessful because of the effects of attenuation. The UltraVision 1.2R4 software suite was used to generate specific delay laws for each of the 22 elements of both the SN1 and SN2 arrays, such that target depth focuses of 25.4, 50.8, and 76.2 mm (1.0, 2.0, and 3.0 in.) at 0° (azimuthal) could be achieved. The nanosecond delays are precisely timed so that the contribution from each individual element can constructively interfere with the other elements producing a sound beam maximum at a particular angle and depth. The reception pin-ducer was positioned at the depth of the focal plane and raster scanned. The raster scans were spatially encoded with a resolution of 0.25 mm (0.01 in.) in the scan direction and for a scan length of 80 mm (3.1 in.) and 0.5-mm (0.02-in.) resolution in the index axis for a length of 100 mm (3.9 in.). Figures 6.11 and 6.12 show the 76.2-mm (3-in.) focused beam at 0° for both SN1 and SN2 prototype probes, respectively. The fiducial marker is circled in red. The right-hand side of the figure shows the focal spot (see red/orange color) in the center of the array at the correct position of 0° and that it is highly symmetrical in the primary axis (vertical). Table 6.4 provides the dimensional data associated with the active and passive sound field dimensions for both probes as a function of focal depth.

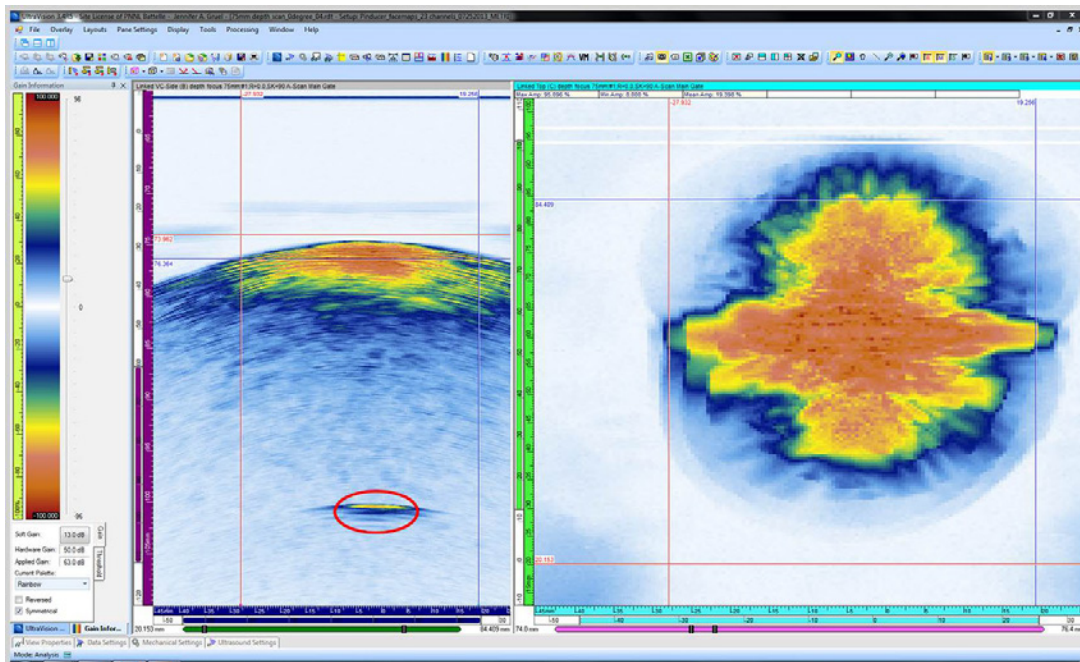


**Figure 6.11.** 0° Depth Focus at 76.2 mm (3 in.) for the SN1 Prototype Probe. Red circle indicates the fiducial response.

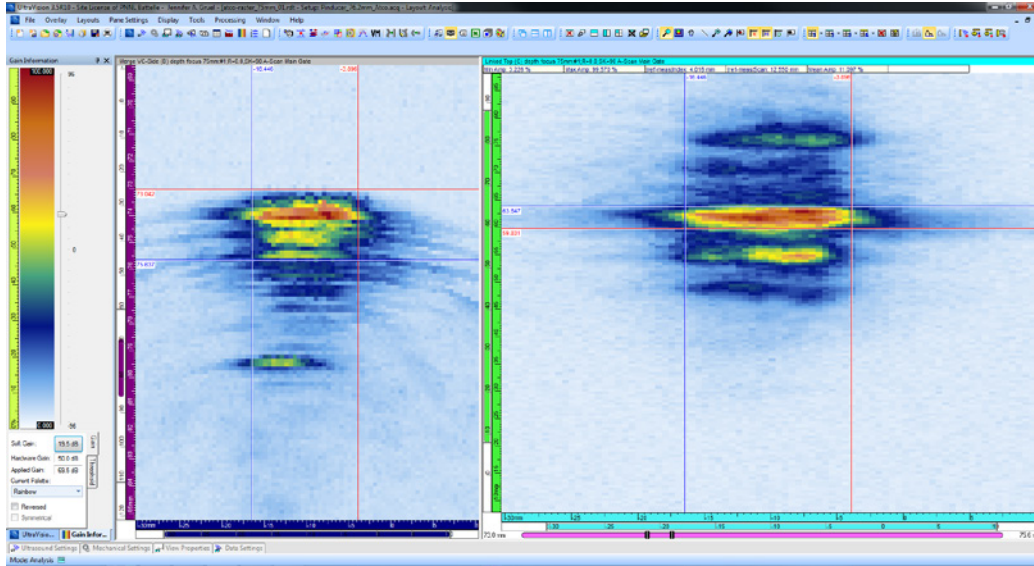


**Figure 6.12.** 0° Depth Focus at 76.2 mm (3 in.) for the SN2 Prototype Probe. Red circle indicates the fiducial response.

**Table 6.4. Passive and Active (length and width) Sound Field Dimensions as a Function of the Focal Depth, at -6 dB Points, for both the SN1 and SN2 Prototype Probes**

Probe	Focal Depth		-6 dB				-12 dB			
			Length (passive)		Width (active)		Length (passive)		Width (active)	
	(mm)	(in.)	(mm)	(in.)	(mm)	(in.)	(mm)	(in.)	(mm)	(in.)
SN1	25.4	1.0	26.1	1.0	7.0	0.3	30.1	1.2	13.1	0.5
	50.8	2.0	26.1	1.0	5.5	0.2	32.1	1.3	10.0	0.4
	76.2	3.0	28.6	1.1	7.5	0.3	38.7	1.5	10.5	0.4
SN2	25.4	1.0	14.1	0.6	4.5	0.2	20.6	0.8	8.5	0.3
	50.8	2.0	13.1	0.5	4.5	0.2	20.6	0.8	6.0	0.2
	76.2	3.0	12.6	0.5	4.0	0.2	20.1	0.8	5.5	0.2

From an analysis of Table 6.4, it is seen that probe SN2 sound field dimensional values decrease as the focal depth of the probe increases, which is what would be expected for a probe designed to have a focal depth range of 75 mm to 110 mm with a suitable depth of focus. The SN1 probe dimensions do not trend in this manner, and their values are approximately a factor of two larger than the SN2 probe values, indicating a generally wider sound field. This is, in part, attributed to the differences in operational frequency between the two probes.

### 6.1.5 Evaluation of Selected Angles

Similar to the evaluation of depth focusing capabilities of both SN1 and SN2 22-element arrays, the angle evaluation shows beam formation at a specified depth and azimuthal angle for each probe. The UltraVision 1.2R4 software suite was used to generate specific delay laws for each of the 22 elements of both arrays such that angles of 5, 10, 15, and 20° azimuthal at a constant target depth of 50.8 mm (2 in.) were formed. The nanosecond delays are precisely timed so that the contribution from each individual element can constructively interfere with the other elements producing a sound beam maximum at the particular angle and depth. The reception pin-ducer was positioned at the depth of the focal plane and raster scanned. The raster scans were spatially encoded with a resolution of 0.25 mm (0.01 in.) in the scan direction and for a scan length of 50 mm (2 in.) and 0.5-mm (0.02-in.) resolution in the index axis for a length of 100 mm (3.9 in.). Figures 6.13 and 6.14 illustrate the 15° azimuthal beam focused at 50.8 mm (2 in.) for the SN1 and SN2 prototype probes, respectively. The fiducial marker is circled in red. The position of the focal spot center has shifted upward (in the vertical direction) from its zero location. This indicates that the array is steering the focal spot position and that it is steering in the right direction. The maximum energy in the focal spot is clearly concentrated at the topmost portion. Figures 6.13 and 6.14 also show that as a result of steering, the beam width has increased. This behavior was modeled during the design phase and is a well-known behavior of phased arrays. The data collected during this test could be used to estimate the location of the beam center for each of the steering angles, perform a calculation for an estimate of the actual steering angle achieved, and compare this result to the intended steering angle. The purpose of this test was to qualitatively assess the beam steering capability of the probe (which was confirmed), and there was a level of difficulty of determining an exact center of the focal spot of a steered beam; therefore, no quantitative analysis of the data was conducted.

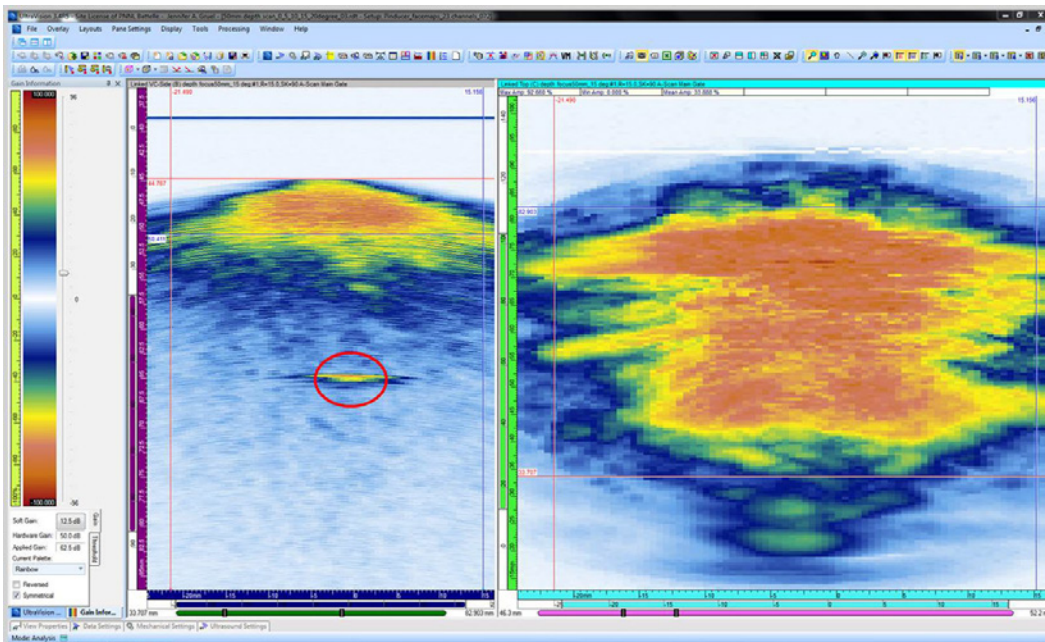


**Figure 6.13.** 15° Azimuthal at a Depth Focus at 50.8 mm (2 in.) for the SN1 Prototype Probe. Red circle indicates the fiducial response.

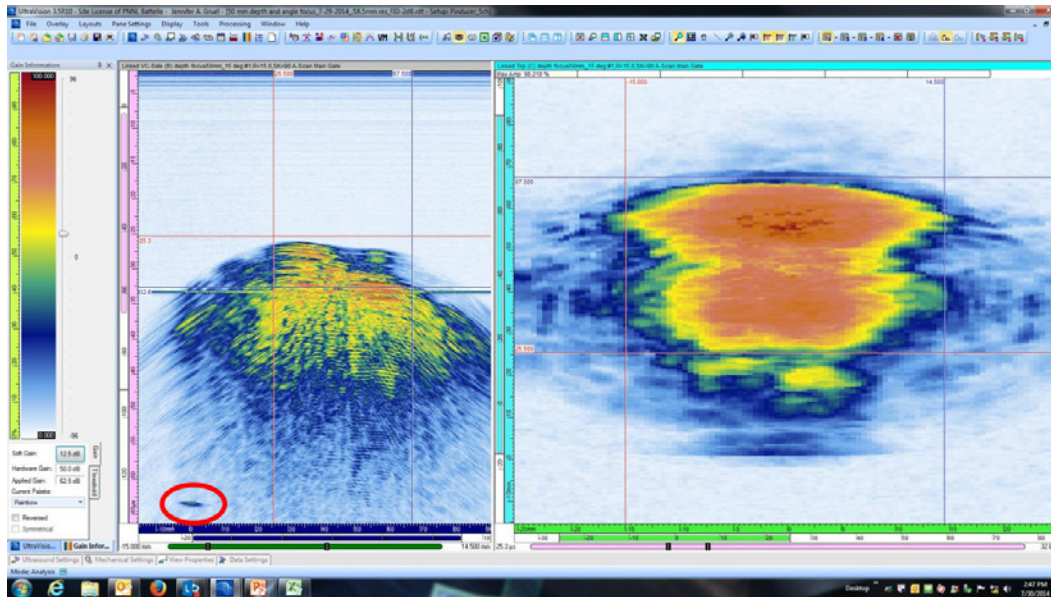


**Figure 6.14.** 15° Azimuthal at a Depth Focus at 50.8 mm (2 in.) for the SN2 Prototype Probe. Red circle indicates the fiducial response.

From an analysis of the data over the span of angles tested, 0°, 5°, 10°, 15°, and 20°, both SN1 and SN2 prototype probes showed effective off-axis beam steering capability as per the design of both probes.

## 6.2 Post-Fabrication Assessment of Temperature Resistance and Thermal Cycling Effects (in Hot Oil)

This subsection describes post-fabrication testing of the temperature resistance and thermal cycling effects on both SN1 and SN2 probes in hot oil. The prototype probes were immersed in hot oil to test their durability and operability as a function of temperature and time. The digital photo in Figure 6.15 illustrates the laboratory configuration used to conduct the evaluation. While the tests were conducted in a fume hood, refined avocado oil was used as the medium to conduct these tests. This oil was chosen because of its high smoke point of 271°C and a flash point of greater than 338°C.



**Figure 6.15.** Photograph of the Laboratory Fume Hood Enclosure, Housing the Heating Plate/Oil Bath, the Prototype Probe, the Associated Manipulation Apparatus, and the Measurement Instrumentation

Both prototype probes (SN1 and SN2) were immersed in this bath of oil at room temperature (approximately 20°C). The probes were manipulated (perpendicular) to a specified distance of 50.8 mm (2.0 in.) from Target #1 (described in detail in the FY13 TLR) as it lay on the bottom surface of the oil-bath container (Braatz et al. 2013). Target #1 (included an 11-mm high pin and a backwall surface) provided the reflecting surfaces, as the probe was kept in an operational mode throughout the heating process. Time-encoded data were acquired, and the reflected signal responses as a function of time in the oil bath were captured at various temperature/time points over the duration of the tests. The PA-UT instrumentation and data acquisition computer were located outside the fume hood where the ultrasonic data were monitored and captured. Measurements were obtained at 20, 75, 125, 175, 225, and 260°C. The ramping up of the temperature was a time-consuming process, taking between 3 and 4 hours per test. Analysis of the ultrasonic echo from Target #1 on the bottom of the containment was used to determine if the probe had experienced any damage or was otherwise impeded from operating effectively because of temperature-induced effects. The ultrasonic image provided in Figure 6.16 illustrates an example of the pin and backwall signal response used for assessing probe functionality and operability during these temperature tests. Because the acoustic velocity of the oil will change with temperature, the only changes identified in the signal were from shifts in the time-of-flight of the backwall echo as the temperature increased from 20°C to 260°C. All tests were conducted without moving the probe at all. The prototype probes were positioned over one of the vertical pin targets (on Target #1), and both the top of the 11-mm pin as well as the target base (backwall) signal can be seen in the volume-corrected sectorial view shown in Figure 6.16. As a result of these tests, there was no indication that the 260°C temperature, nor the thermal cycling from room temperature up to the high point of 260°C, had any negative effects on probe integrity or performance.

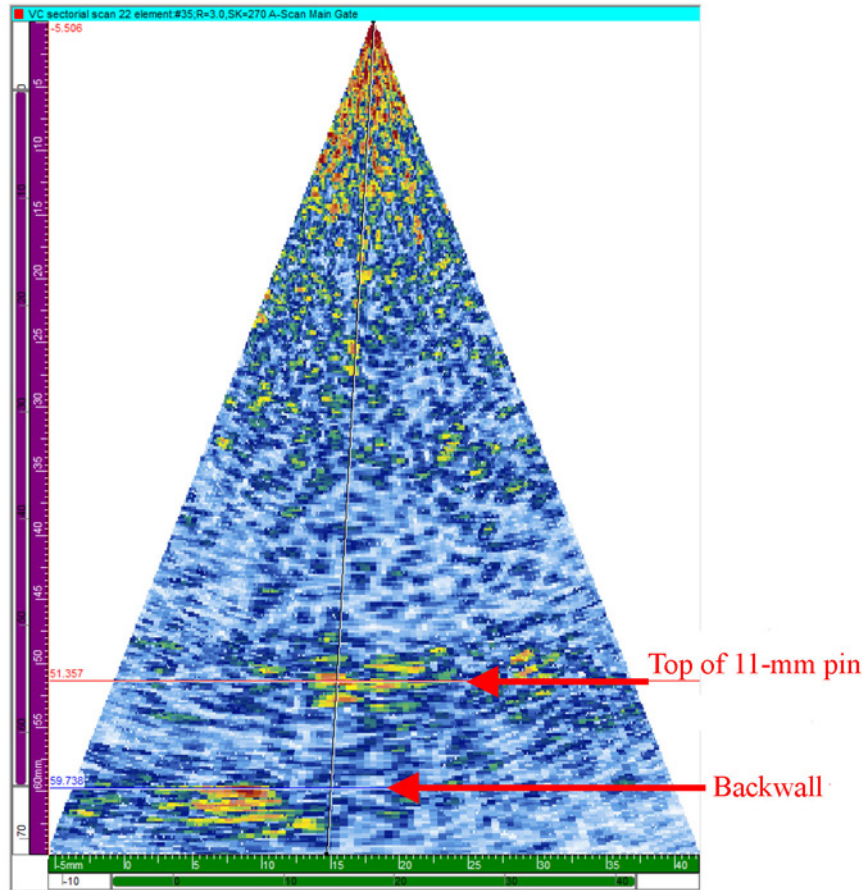


**Figure 6.16.** PA-UT Image (volume-corrected sectorial view) Illustrating the 11-mm Pin and Backwall Signal Responses from Target #1 on the Bottom of the Hot-Oil Container at 260°C, Obtained from the SN2 Probe, and Monitored During Thermal Cycling and Resistance Tests

### 6.3 Element-by-Element, Pulse-Echo, Ultrasonic Signal Responses for SN1 and SN2 Prototype Probes (in Water)

This subsection describes post-fabrication testing of both SN1 and SN2 prototype probes on an element-by-element basis. The analysis is conducted from evaluating the individual voltage responses from each element after employing a standard excitation pulse, and capturing the reflected signal response from a polished, fused silica reflector plate (conducted in pulse-echo mode, without the use of a separate pin-ducer for receiving signal responses). Figure 6.17 provides a digital photograph illustrating the laboratory measurement setup for obtaining ultrasonic signal responses from the fused silica reflector in water.

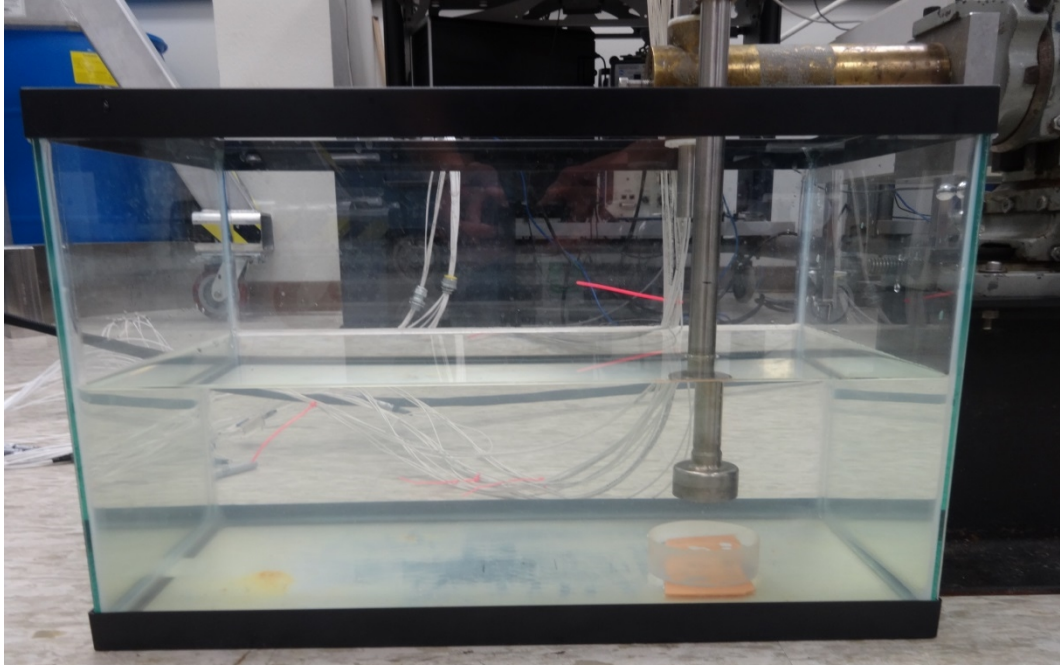


**Figure 6.17.** Photograph of the Laboratory Configuration for Capturing Ultrasonic Signal Responses for Assessing the Pulse-Echo Waveform Characteristics (time, amplitude, and frequency) from a Standard Flat Target

Each individual element of both the SN1 and SN2 prototype probes was excited in a pulse-echo mode using a 250-ns square-wave pulse, and the reflected signal response from each element was captured. The waveforms were sampled at a 50-MHz digitizing frequency, and averaged 16 times prior to data capture, to reduce electronic noise. The quartz block was used as the standard reflector using a water path (standoff distance) of 25.4 mm (1.0 in.) between the probe face and the fused quartz block. Data were analyzed in both the time and frequency domains for each probe. The detailed analysis is provided in Subsection 6.3.1.

### **6.3.1 Individual Element, Frequency Response Analysis, and Bandwidth Calculations for SN1 and SN2 Prototype Probes**

This subsection describes post-fabrication assessments of the center and peak frequency responses from the FFTs of individual element responses captured and evaluated in Subsection 6.3. In addition, a description of the post-fabrication assessments of the  $-6$  dB BWs of each element in both SN1 and SN2 prototype probes, from the FFTs of individual element responses, are analyzed and discussed here. Figures 6.18 and 6.19 provide example rf waveforms (time-series) and frequency spectra (from FFTs) for the same individual element signal response for the SN1 and SN2 prototype probes, respectively. Each element was evaluated individually, and resultant data and calculations for bandwidth from this assessment are provided in Table 6.5.

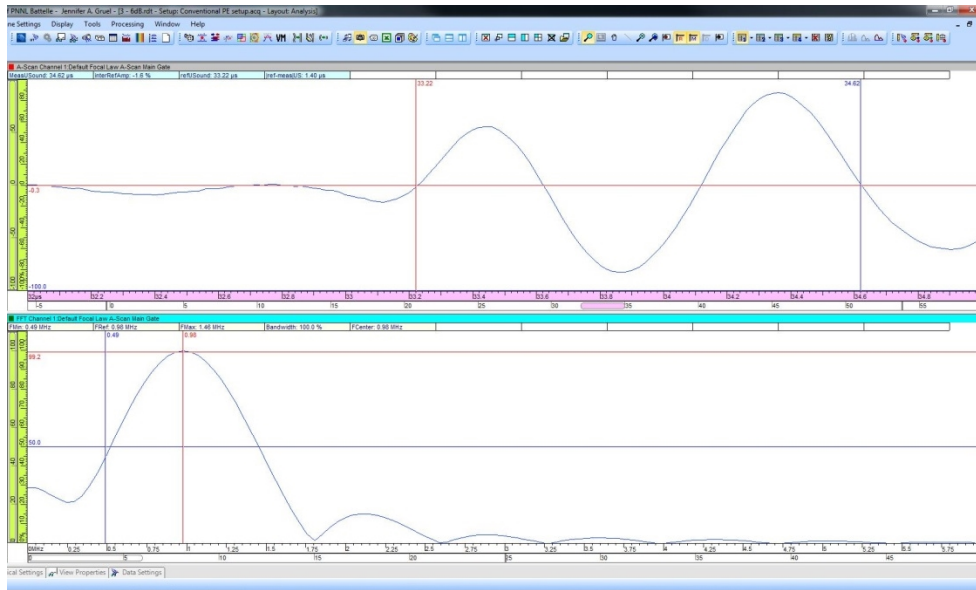


**Figure 6.18.** Top: A-scan, rf Waveform (amplitude versus time-series) of the First Arrival of the Ultrasonic Signal Response from the Fused Silica Reflector Block, for the SN1 Probe, Element #3. Bottom: The FFT of the Time-Gated Portion of the Waveform in the Top View.

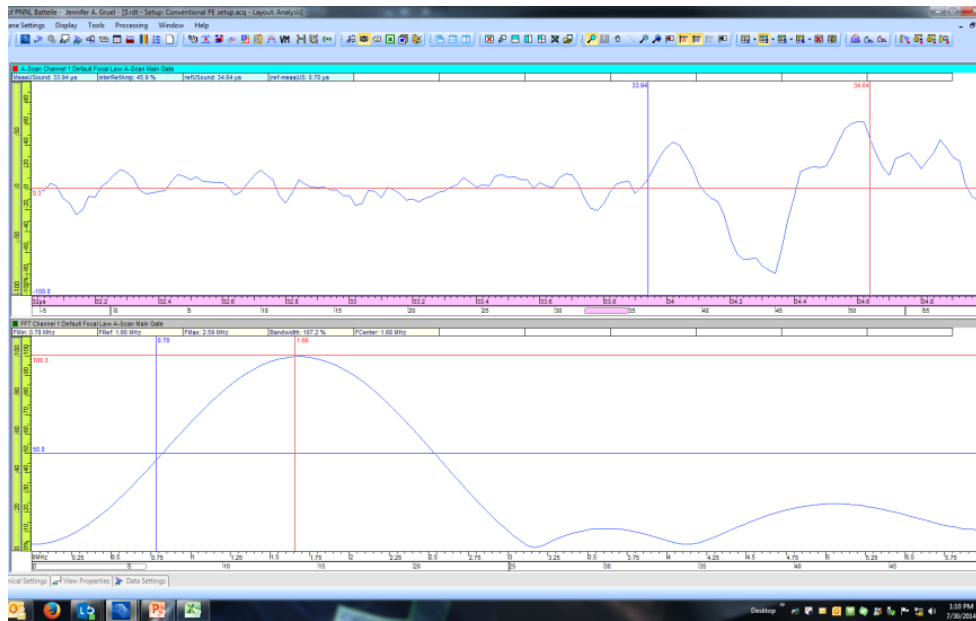


**Figure 6.19.** Top: A-scan, rf Waveform (amplitude versus time-series) of the First Arrival of the Ultrasonic Signal Response from the Fused Silica Reflector Block, for the SN2 Probe, Element #3. Bottom: The FFT of the Time-Gated Portion of the Waveform in the Top View.

The effort focused on evaluating the individual signal responses as a function of amplitudes and frequency characteristics from the FFTs for each rf waveform. A standard time-window was used to capture the 1<sup>st</sup> arrival portion of the rf-waveform response (sampling a minimum of 1½ cycles), and each individual FFT was then computed. From the FFTs, peak and center frequencies were documented and the 6 dB magnitude and frequency points (both upper and lower points) were recorded as per the guidance in ASTM E-1065. Bandwidth calculations were made for both the SN1 and SN2 probes, and are presented in Table 6.5.

**Table 6.5.** Element-by-Element Data and Calculations Resulting from the Frequency Response Analysis of Signal Responses from the SN1 and SN2 Prototype Probes, Captured from Immersion Testing in Water Using a Standard Reflector

Element #	SN1					SN2				
	F Peak (MHz)	F Center (MHz)	-6 dB Lower (MHz)	-6 dB Upper (MHz)	BW (%)	F Peak (MHz)	F Center (MHz)	-6 dB Lower (MHz)	-6 dB Upper (MHz)	BW (%)
1	0.98	0.98	0.49	1.46	100	1.56	1.54	0.20	2.88	175
2	0.98	0.98	0.49	1.46	100	1.17	1.25	0.29	2.2	153
3	0.98	0.98	0.49	1.46	100	1.66	1.68	0.78	2.59	107
4	0.98	0.98	0.49	1.46	100	1.42	1.42	0.49	2.34	131
5	0.98	0.98	0.49	1.46	100	1.56	1.61	0.83	2.39	97
6	0.98	0.98	0.49	1.46	100	1.66	1.68	0.78	2.59	107
7	0.98	0.98	0.49	1.46	100	1.61	1.64	0.78	2.49	105
8	0.98	0.98	0.49	1.46	100	1.66	1.68	0.78	2.59	107
9	0.98	0.98	0.49	1.46	100	1.61	1.64	0.78	2.49	105
10	0.98	0.98	0.49	1.46	100	1.61	1.64	0.78	2.49	105
11	1.17	1.20	0.63	1.76	95	1.61	1.61	0.68	2.54	115
12	0.98	0.98	0.49	1.46	100	1.27	1.27	0.54	2	115
13	0.98	0.98	0.49	1.46	100	1.61	1.66	0.78	2.54	106
14						1.61	1.66	0.78	2.54	106
15	1.27	1.42	0.39	2.44	144.8	1.61	1.61	0.73	2.49	109
16	1.07	1	0.24	1.76	151.2	1.66	1.68	0.78	2.59	107
17	0.98	0.98	0.49	1.46	100	1.66	1.71	0.83	2.59	103
18	0.98	0.98	0.49	1.46	100	1.51	1.56	0.73	2.39	106
19	1.07	1.07	0.49	1.66	109.1	1.61	1.66	0.78	2.54	106
20	1.27	1.34	0.68	2	98.2	1.86	1.88	0.98	2.78	96
21	1.32	1.34	0.68	2	98.2	1.66	1.71	0.83	2.59	103
22	0.98	0.98	0.54	1.42	90	1.56	1.64	0.78	2.49	105
Average	1.04	1.05	0.50	1.59	104.10	1.58	1.61	0.71	2.51	112.18
Standard Deviation	0.11	0.14	0.09	0.26	14.63	0.14	0.14	0.18	0.17	17.95

## 6.4 Element-by-Element Sensitivity Analysis for SN1 and SN2 Prototype Probes

This subsection describes post-fabrication testing and analysis of the sensitivity variations (in normalized % amplitude) from element-to-element, of both SN1 and SN2 prototype probes, from pulse-echo modality data obtained and discussed in Subsection 6.3.

Data were collected from individual element responses off of a flat quartz reflector 25.4 mm (1 inch) away in water. Table 6.6 provides the data for individual elements of both probes. Maximum amplitude responses from the quartz reflector were normalized to 5 dB for each element so that a comparison could be made among elements from both SN1 and SN2 prototype probes. Five dB was chosen because it was the minimum amount of amplification required among all elements for the ultrasonic response from the quartz block to be detected (above background noise). The variation in sensitivity from element-to-element for each probe is illustrated in Figure 6.20.

**Table 6.6.** Signal Response Data from a Quartz Reflector Block, for Assessment of Element-to-Element Sensitivity Between SN1 and SN2 Prototype Probes

Element #	SN1		SN2	
	Total Applied Gain (dB)	Normalized Amp (%)	Total Applied Gain (dB)	Normalized Amp (%)
1	6	51.07	28	0.63
2	6	51.87	6	46.70
3	6	49.82	28	0.55
4	6	51.34	5	52.10
5	6	49.73	28	0.74
6	6	51.51	28	1.73
7	6	51.60	28	0.70
8	6	50.80	28	0.82
9	6	51.25	28	1.02
10	6	51.16	28	0.71
11	28	4.70	28	0.96
12	6	50.71	10	26.26
13	6	50.44	28	1.40
14			28	1.00
15	28	5.80	28	1.37
16	28	1.88	28	1.25
17	6	51.69	28	1.85
18	6	51.34	26	3.07
19	28	2.86	28	2.61
20	20	14.35	28	1.42
21	20	15.54	28	1.82
22	28	6.75	28	1.49
Average	12.00	34.83	25.05	6.83
Standard Deviation	9.67	21.67	7.23	14.46

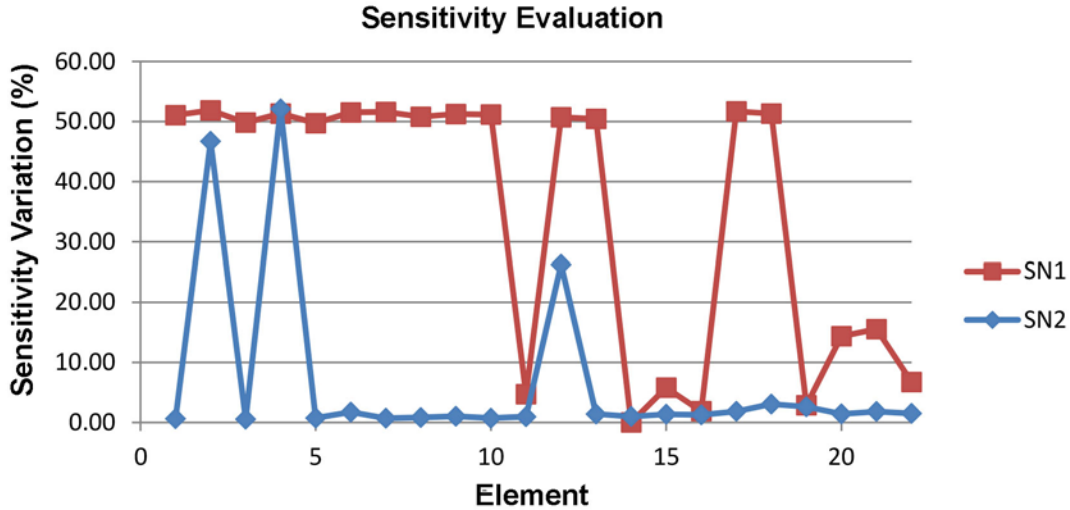


**Figure 6.20.** Element-by-Element Sensitivity Variation between Both SN1 and SN2 Prototype Probes

An analysis of Table 6.6 and Figure 6.20 shows significant variability in sensitivity between elements of the two probes. In general, the SN1 probe appears to have more elements that are “hotter” than the SN2 probe. These hotter elements require less gain to acquire the same signal response (in amplitude) than that of their SN2 element counterparts. Table 6.6 indicates a factor of approximately 5 in amplitude sensitivity difference between SN1 and SN2 probes, corresponding to a nearly 13 dB difference in the required gain levels to operate these probes at equivalent amplitude levels.

## 6.5 Sound Field Dimensional Characterization Analysis for SN1 and SN2 Prototype Probes

This subsection describes post-fabrication testing and analysis of sound field mapping data obtained in water, for both the SN1 and SN2 prototype probes. Sound field dimensions (focal spot size) at  $-6$  dB and  $-12$  dB points at a nominal distance from the face of the probe in water, using a pin-ducer receiving probe, will be presented, compared, and discussed.

From a review of subsection 6.1.4 and the data provided in Table 6.4, it is clear that the sound field dimensions for the focal “spot” size of the two 22-element prototype arrays are significantly different. But the trend, as a function of focal depth and as a function of the amplitude envelope of the sound field ( $-6$  dB versus  $-12$  dB), indicates that the SN1 probe has a sound field that is generally twice that of the SN2 probe in both passive and active element dimensions (length and width, respectively).

The SN1 prototype showed that in the passive (length) dimension of the probe, the sound field slightly increased in size as the focal depth increased. For the SN2 prototype, the trend was in the opposite direction, showing that as the focal depth increased from 25.4 mm up to 76.2 mm, the focal dimensions decreased in the passive (length) axis. For the SN2 probe, this same trend is generally true for the dimensions in the active (width) axis as well. This shows that the SN2 probe produces a sound field with a smaller dimensional footprint than the SN1 probe. By design, both probes were fabricated to

generate a more localized focal spot size over a range of depths from approximately 75 mm (2.95 in.) to approximately 110 mm (4.33 in.), with a depth of focus of nearly 50 mm at the 6 dB points. The modeling results from simulations of the 22-element array prototype design are provided in the FY13 TLR (Braatz et al. 2013). While neither probe appears capable of generating the dimensions calculated by the model, the SN2 probe has a much tighter focal spot size than the SN1 probe at the same focal depth, in both axes. In theory, this should translate into the capability to provide a sharper, cleaner image of objects in comparison to the SN1 probe, at the same distance.

## 6.6 Spatial Resolution Analysis for SN1 and SN2 Prototype Probes

This subsection describes post-fabrication testing of both SN1 and SN2 prototype probes, focused on the acquisition of ultrasonic data describing the spatial resolution performance for these ETUs. Spatial resolution data and testing procedures using raster scanning of the probe and employing flat reflectors with various spacings to evaluate array resolution performance in water are presented. Sound field dimensional analysis is presented and a comparison of the spatial resolution performance of each probe will be discussed.

A simple resolution target was built from a  $\frac{3}{4}$ -in. thick Plexiglas plate. A set of 0.5-in. deep threaded holes were tapped into the plate to allow for the placement of six pairs of 1.5-in. hex socket-head cap screws, placed at different distance spacings from one another. All screws were 28.57 mm (1.125 in.) above the Plexiglas backwall. Each pair of screws was separated 25.4 mm (1.0 in.) apart from the next pair. The pair with the widest center-to-center separation had a distance of 25.4 mm (1.0 in.). The next closest pair was 19.05 mm (0.75 in.), and in descending distance order, subsequent pairs were spaced at 12.7 mm (0.5 in.), 10.16 mm (0.4 in.), 7.62 mm (0.3 in.), and 6.35 mm (0.25 in.), respectively. The screw heads were filled with epoxy and surfaced to provide a flat reflector with a nominal diameter of 5.72 mm (0.225 in.). A digital photo of the target is provided in Figure 6.21.



**Figure 6.21.** Photograph of the Resolution Target Used to Assess Imaging Resolution Characteristics between SN1 and SN2

Both SN1 and SN2 probes were used in identical fashion during the scanning of this resolution target. The water path was set at 76.2 mm (3.0 in.) from the target plane with the appropriate focal laws in place, for optimal imaging of the screw caps. The depth of focus provided an ample signal response off the Plexiglas plate, for a constant background signal response. Both probes were scanned in a raster pattern over the resolution target at a standoff distance of 76.2 mm (3 in.) in water. The raster scans used a  $0.3 \times 0.3$  mm ( $0.012 \times 0.012$  in.) resolution scan pattern. The PA-UT images for each probe were evaluated, and a dimensional analysis was conducted to determine the resolving capability of each probe. The SNR for each probe was also computed from the resultant images. Figures 6.22 and 6.23 illustrate the PA-UT images, including a time-gated C-scan view (X-Y axis, top-down composite view of the screw-cap reflectors) for the SN1 and SN2 prototype probes, respectively.

The wavelength ( $\lambda$ ) in the material is determined by the relationship:  $\lambda = c / f$ , where  $c$  is the acoustic velocity and  $f$  is the frequency. Typical units for acoustic velocity are m/s or in./ $\mu$ sec. In water, the acoustic velocity at room temperature is 1486 m/s, or 0.0584 in./ $\mu$ sec. The operational frequencies of the probes (from the discussion in subsection 6.3.1) differ, based on the differences in fabrication processes used. From this earlier discussion, the SN1 probe has an average operational frequency of 1.05 MHz, while the SN2 probe has an average operational frequency of 1.61 MHz. This translates into a wavelength of 1.42 mm (0.056 in.) for the SN1 probe and 0.92 mm (0.036 in.) for the SN2 probe in water. Advanced PA-UT imaging systems can theoretically generate images with an optimal resolution of half a wavelength ( $\frac{1}{2} \lambda$ ). Therefore, ideally, a well-designed and effectively optimized PA-UT probe at a 2-MHz operating frequency using the longitudinal wave mode, could potentially resolve reflectors on the order of 0.372 mm (0.0146 in.) in size, if designed properly and if employed with the appropriate focal laws and signal processing algorithms, where attenuation is minimal. In our case, sodium is more attenuative to the ultrasonic energy than water, and these prototype PA-UT probes have room for improvement with regard to fabrication specifications and processes.

From a review of the data acquired from the resolution target standard, the SN1 probe is capable of resolving the two individual screw cap reflectors at a separation distance of 7.62 mm (0.3 in.), but is unable to resolve the reflectors that are separated by 6.35 mm (0.25 in.). The SN2 probe is capable of resolving the reflectors that are separated by 6.35 mm (0.25 in.). It is not clear as to why the previous pair of reflectors are not well resolved in the SN2 image of Figure 6.23, but this could be attributed to differences in the  $0^\circ$  alignment of the probe, perpendicular to the target, and also the rotational alignment of the array relative to the target standard. The image in Figure 6.22 shows that the SN1 probe appears to be ideally aligned to the reflector standard in the immersion tank, while there appears to be a smearing effect and slight directional bias of the image in Figure 6.23 for the SN2 probe. Regardless, both probes have suitable resolving power, based on the original design specifications; and it appears that the SN2 probe has a slightly improved resolution capability over that of the SN1 prototype probe.

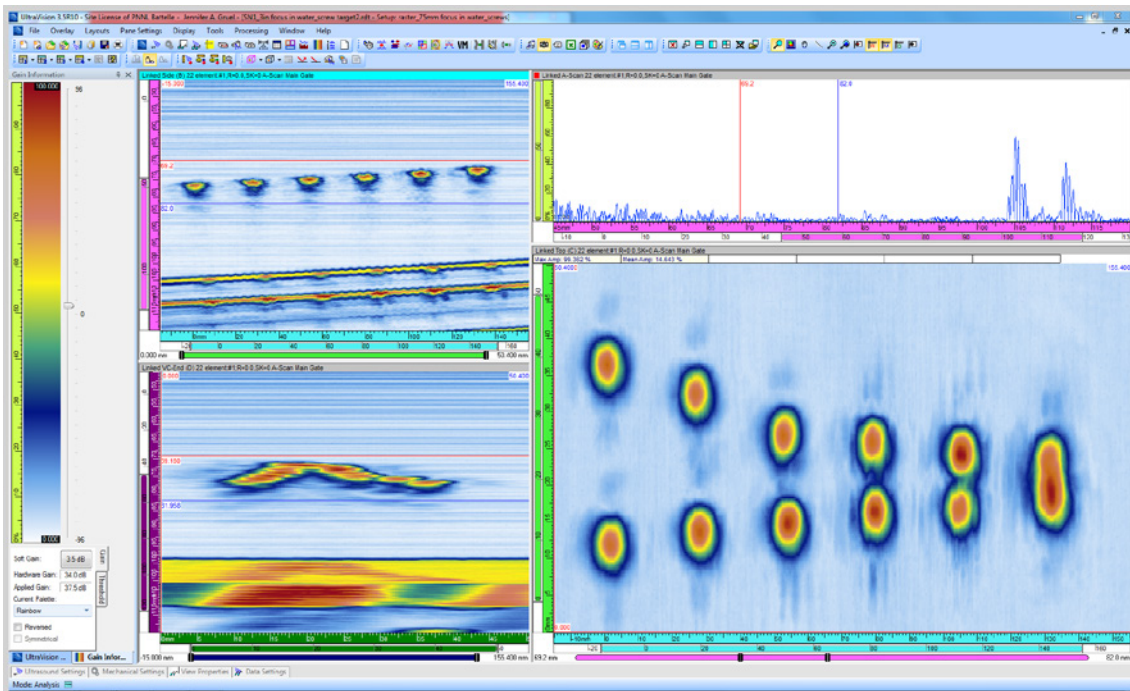


**Figure 6.22.** PA-UT Image of the Resolution Target Using the SN1 Probe in Water at a Focal Distance of 76.2 mm (3.0 in.)

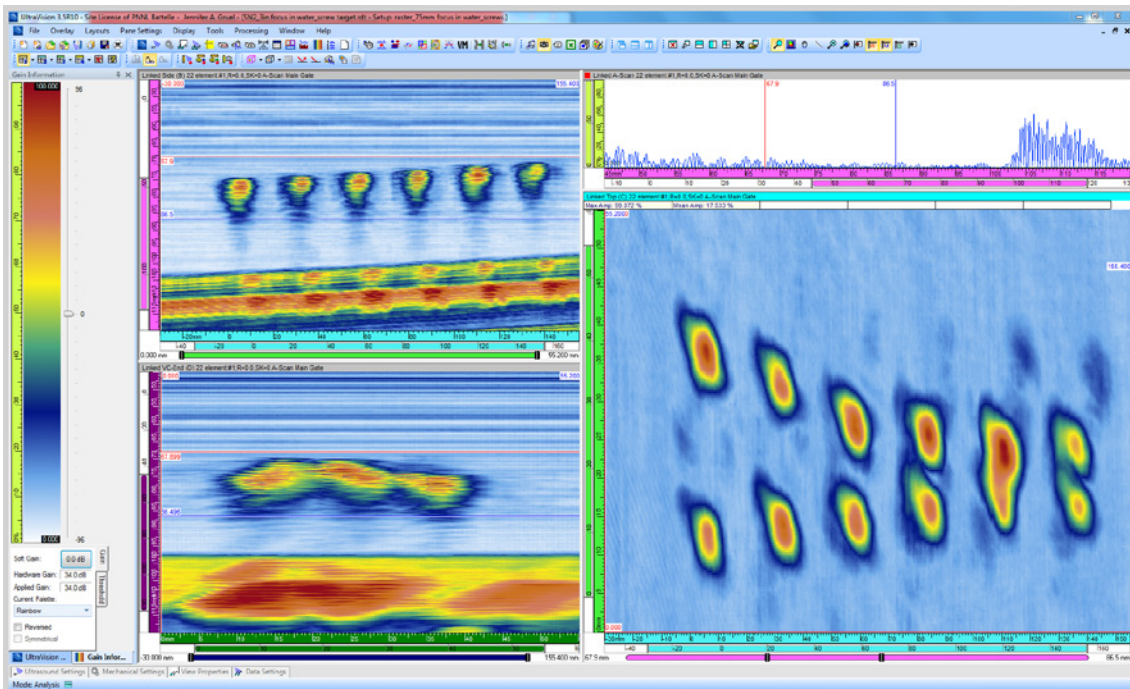


**Figure 6.23.** PA-UT Image of the Resolution Target Using the SN2 Probe in Water at a Focal Distance of 76.2 mm (3.0 in.)

Table 6.7 provides the as-built dimensions and spacings of the resolution target, as well as the ultrasonically measured dimensions resulting from the SN1 and SN2 scans. The measured dimensions were quite accurate, relative to the true state. As can be seen from the data in Table 6.7, as the probe approaches its resolution limit, the dimensional measurement accuracy begins to decrease. However, discrete and separate signal responses can still be easily detected and resolved by the SN2 probe for the closest spaced reflectors.

**Table 6.7.** True-State Dimensions of the Resolution Target Reflectors and Ultrasonically Measured Separation Dimensions from the PA-UT Data Obtained from SN1 and SN2 Probes

	Resolution Target Reflector Set (Screw Pairs)						Mean Spacing Between Sets, mm (in.)
	1 mm (in.)	2 mm (in.)	3 mm (in.)	4 mm (in.)	5 mm (in.)	6 mm (in.)	
As-built Spacing (True State)	25.4 (1.00)	19.05 (0.75)	12.7 (0.50)	10.16 (0.40)	7.62 (0.30)	6.35 (0.25)	25.4 (1.00)
SN1 (Measured)	24.62 (0.97)	18.69 (0.74)	12.09 (0.48)	9.32 (0.37)	7.5 (0.30)	N/A	26.1 (1.03)
SN2 (Measured)	23.72 (0.93)	18.32 (0.72)	12.63 (0.50)	9.67 (0.38)	7.21 (0.28)	8.24 (0.32)	26.18 (1.03)

## 6.7 SNR Assessment for SN1 and SN2 Prototype Probes

This subsection describes an analysis of the SNR data for both SN1 and SN2 probes, computed from both pre-fabrication and post-fabrication performance and functional testing protocols. An evaluation of SNR for the individual elements of these two probes will be discussed.

From a review of the comparative analysis conducted for both probes, we can say that during the pre-fabrication testing of the elements, the SNR was generally 8–10 dB higher for the SN2 prototype array on an element-to-element basis in comparison to the SN1 probe. This corresponds to a voltage ratio enhancement of between 2.5-to-1 and 3.2-to-1 for the SN2 probe SNR over that of the SN1 probe. After fabrication and housing of the probe, the SNR values of the two probes appear to converge. From the reflector data obtained in water and described in Section 6.6, the SNR for the SN1 probe was 16.1 dB and the SNR for the SN2 probe was 8.5 dB. This corresponds to an approximate difference of 7.6 dB, which corresponds to a voltage ratio difference of 2.4-to-1. The SN1 probe demonstrated a superior post-fabrication SNR level, over that of the SN2 probe, even with element #14 being disabled.



## 7.0 Discussion and Conclusions

This TLR provides an evaluation of data from both SN1 and SN2 prototype probes that establishes a foundation for comparing and contrasting the performance of these probes. This assessment does not include performance of the probes in-sodium, but focuses on the performance characteristics via direct measurements obtained prior to housing the elements, after housing the elements, in water, and finally, in hot oil.

The Technical Team assessed both probes using equivalent performance and operational parameters. A set of pre-fabrication pulse-echo tests on individual array elements (in water) were conducted, followed by a set of post-fabrication pulse-echo testing on individual array elements, also in water. This included measurements to validate the array pin connections, the transmit uniformity for each element, the cross-talk (to assess inter-element coupling between neighboring elements), and an evaluation of selected depth focus points and angles (to assess how effectively the probe can skew the sound field off its 0° primary axis). Additionally, an assessment of temperature resistance and thermal cycling effects (in hot oil) was conducted. A number of laboratory measurements and performance characterization scans were conducted to quantify a set of critical attributes used as metrics for assessing and comparing probe performance and capabilities. Key efforts included the acquisition of:

1. Individual voltage responses from each element after employing a standard excitation pulse, and reflected from a polished, fused silica reflector plate (conducted in pulse-echo mode, without the use of a separate pin-ducer for receiving signal responses)
2. Center and peak frequency responses from the FFTs of individual elements
3. -6 dB BWs of each element
4. Sensitivity variations (in normalized % amplitude) from element-to-element
5. Sound field dimensions (focal spot size) at -6 dB and -12 dB points at a nominal distance from the face of the probe in water, using a pin-ducer receiving probe
6. Spatial resolution testing using raster scanning of the probe and employing flat reflectors as with various spacings to evaluate array resolution performance in water
7. Evaluation of signal-to-noise ratio (SNR) from both pre-fabrication testing of the individual elements and post-fabrication tests.

With the analyses of data obtained from these performance characterization tests, the PNNL Technical Team was able to quantify key performance parameters that can be compared and contrasted between the two ETU probes, SN1 and SN2. In particular, sound field dimensions (spot size), resolution capabilities, SNR, frequency response, and BW characteristics constitute the suite of critical attributes used to evaluate these probes.

From a review of the data provided in Sections 5.0 and 6.0, it is clear that the various stages of fabrication and the materials and quality of the processes employed for construction of the elements, backing, soldering, and bonding, all can critically impact probe performance. Prior to fabrication of the housed probe arrays, it was shown that the SN2 probe had significantly lower noise levels and an improved SNR for the individual elements over that of the SN1 probe; on the order of 8–10 dB. After

fabrication as each element was being validated for connectivity, the Team found that all 22 elements were confirmed to be operational for both probes at the time these data were taken; however, some elements had significantly reduced activity. Element #14 was found to be non-operational for the SN1 probe during the late FY14 portion of the performance characterization tests.

An assessment of the transmit uniformity on an element-by-element basis was conducted, and these measurements established a foundation for assessing areas of the arrays that were not emitting energy in an efficient manner, or where areas were dis-bonded. The SN1 array clearly illustrated areas of complete dis-bonding where no ultrasonic energy was being emitted, but this did not have a significant effect on the overall performance of the probe, in comparison to the SN2 probe. While the overall activity of all elements of the SN2 probe was demonstrated, and there was no evidence of dis-bonding over the aperture of the SN2 array, it was noted that there were elements that emit more acoustic energy than others across the 22 elements of the SN2 array. Laboratory measurements provided valuable dimensional data associated with the sound fields, and an assessment of the element-to-element cross-talk showed that inter-element ultrasonic leakage was more effectively isolated for the SN2 probe over that of the SN1 probe ( $-13$  dB as opposed to  $-7$  dB), but there is still much room for improvement. Also, both probes showed suitable capabilities for demonstrating effectiveness at generating sound fields with the appropriate focal depths and dimensions, as well as illustrating the capability to skew their primary sound field lobes over the designed range of angles ( $0^\circ$  to  $20^\circ$ ). This ability to effectively control off-axis beam steering is critical for a PA-UT probe.

In order to assess the effects of temperature and thermal cycling on the probes, both prototype arrays were immersed in hot oil to test their durability and operability as a function of temperature and time. As a result of these tests, there was no indication that the  $260^\circ\text{C}$  temperature, nor the thermal cycling from room temperature up to the high point of  $260^\circ\text{C}$ , had any negative effects on either probe with regard to structural integrity or performance.

Data were acquired to conduct an assessment of the amplitude and frequency response, BW, SNR, and element sensitivity for both probes. Individual voltage responses from each element after employing a standard excitation pulse, and capturing the reflected signal response from a polished, fused silica reflector plate in pulse-echo mode, were analyzed. The results of these tests were somewhat surprising, based upon the in-sodium performance of the SN1 probe in FY13. The most obvious difference of significance between the two probes was the operational frequency. While both prototypes were designed to emit ultrasonic energy and operate at a 2-MHz center frequency, only the SN2 probe was successful at efficiently operating at 2 MHz and above. Both probes have elements that are very broadband, and provide average bandwidths above 100% at the 6 dB points. While the SN2 probe did not quite reach a 2-MHz operating frequency, its BW was broad enough to allow for effective insonification at 2 MHz and beyond, with sufficient ultrasonic energy. In addition, significant variability in sensitivity between elements of the two probes was shown. The SN1 probe had more elements that were “hotter” than the SN2 probe. These hotter elements require less gain to acquire the same signal response (in amplitude) than that of their SN2 element counterparts. This difference in sensitivity was approximately a factor of 5 in amplitude sensitivity between the two probes, corresponding to nearly 13 dB difference in the required gain levels to operate these probes at equivalent amplitude levels. This finding was not anticipated due to the FY13 experiences in-sodium with the SN1 probe.

From an analysis of the sound fields of both probes, it is clear that the sound field dimensions for the focal “spot” size of the two probes are significantly different. The data showed that the SN1 probe has a sound field that is generally twice that of the SN2 probe in both passive and active element dimensions (length and width, respectively). Operational frequency definitely plays a role in this difference. With regard to resolution performance, the SN1 probe is capable of resolving reflectors that are separated by a distance of 7.62 mm (0.3 in.), but is unable to resolve the reflectors that are separated by and 6.35 mm (0.25 in.). The SN2 probe is capable of resolving the reflectors that are separated by 6.35 mm (0.25 in.). Both probes have suitable detection and resolving power, based on the original design specifications, and it appears that the SN2 probe has a slightly improved resolution capability over that of the SN1 prototype probe. Finally, in evaluating the SNR from the data obtained in this study, the SNR for the SN1 probe was 16.1 dB and the SNR for the SN2 probe was 8.5 dB. This corresponds to an approximate difference of 7.6 dB, which corresponds to a voltage ratio difference of 2.4-to-1. The SN1 probe demonstrated a superior post-fabrication SNR level, over that of the SN2 probe, even with element #14 being disabled.

While many key performance parameters and critical attributes exist to quantify the performance of a PA-UT probe, the primary characteristics are those that best describe the capability of a probe to effectively detect, resolve, and characterize the reflectors or anomalies required for identification during an examination. While it has been shown that there are some significant differences between the SN1 and SN2 prototype probes, the Technical Team has been successful at instituting some key improvements to the design and fabrication of the SN2 probe. In some cases, the performance of the SN2 probe is marginally improved over the SN1 probe, and other cases, the performance indicators show that the SN1 probe still has an edge with regard to sensitivity. However, the higher operational frequency and BW of the SN2 probe, coupled with the resolution capabilities of this probe, make it the probe of choice for continued evaluation. In light of the results provided here, PNNL recommends the pursuit of in-sodium testing of the SN2 probe to demonstrate that the next critical challenge is to overcome the wetting issue of the probe in sodium. The Technical Team believes that this issue was at the source of the poor SNR and poor imaging performance of the SN1 probe in FY13, based on discoveries in FY14 with the SN2 probe in-sodium, and the post-sodium performance of the SN1 probe in water and hot oil.



## 8.0 References

ASTM E1065/E1065M-14. 2014. "Standard Practice for Evaluating Characteristics of Ultrasonic Search Units." ASTM International, West Conshohocken, Pennsylvania. DOI 10.1520/E1065-08.

[www.astm.org](http://www.astm.org).

ASTM E2491-13. 2013. "Standard Guide for Evaluating Performance Characteristics of Phased-Array Ultrasonic Testing Instruments and Systems." ASTM International, West Conshohocken, Pennsylvania.

[www.astm.org](http://www.astm.org).

Braatz BG, CL Aardahl, DL Baldwin, AD Cinson, JL Fernandes, AM Jones, PE Keller, MR Larche, R Mathews, CA Mullen, AF Pardini, GJ Posakony, ML Watkins, HT Chien, WP Lawrence, DM Engel and SH Sheen. 2013. *FY2013 Joint Technical Report on Progress in Development of Ultrasonic Under-Sodium Viewing Technology to Enable Inspection Systems for In-Service Inspection and Repair of Liquid Metal Fast Reactors*. PNNL-22872, Pacific Northwest National Laboratory, Richland, Washington.

Watkins ML, BG Braatz, AM Jones, DL Baldwin, GJ Posakony, PE Keller, AD Cinson, MS Prowant, KM Denslow, HT Chien, WP Lawrence, SH Sheen and K Wang. 2012. *Joint Technical Report on Progress in Development of Ultrasonic Under-Sodium Viewing Technology to Enable Inspection Systems for In-Service Inspection and Repair of Liquid Metal Fast Reactors*. PNNL-21853, Pacific Northwest National Laboratory, Richland, Washington.







**Pacific Northwest**  
NATIONAL LABORATORY

*Proudly Operated by **Battelle** Since 1965*

902 Battelle Boulevard  
P.O. Box 999  
Richland, WA 99352  
1-888-375-PNNL (7665)

U.S. DEPARTMENT OF  
**ENERGY**

---

[www.pnnl.gov](http://www.pnnl.gov)